International Journal of Pharmaceutics 582 (2020) 119305

Contents lists available at ScienceDirect

International Journal of Pharmaceutics

journal homepage: www.elsevier.com/locate/ijpharm

Folate decorated polymeric micelles for targeted delivery of the kinase inhibitor dactolisib to cancer cells

Haili Shi, Mies J. van Steenbergen, Bo Lou, Yanna Liu, Wim E. Hennink, Robbert J. Kok*

Department of Pharmaceutics, Utrecht Institute for Pharmaceutical Sciences, Utrecht University, the Netherlands

ARTICLE INFO

Keywords:
Targeted drug delivery
Folate
Polymeric micelles
Dactolisib
Coordination chemistry
Cancer
Signal transduction inhibitor

ABSTRACT

One of the main challenges in clinical translation of polymeric micelles is retention of the drug in the nanocarrier system upon its systemic administration. Core crosslinking and coupling of the drug to the micellar backbone are common strategies to overcome these issues. In the present study, polymeric micelles were prepared for tumor cell targeting of the kinase inhibitor dactolisib which inhibits both the mammalian Target of Rapamycin (mTOR) kinase and phosphatidylinositol-3-kinase (PI3K). We employed platinum(II)-based linker chemistry to couple dactolisib to the core of poly(ethylene glycol)-*b*-poly(acrylic acid) (PEG-*b*-PAA) polymeric micelles. The formed dactolisib-PEG-PAA unimers are amphiphilic and self-assemble in an aqueous milieu into core–shell polymeric micelles. Folate was conjugated onto the surface of the micelles to yield folate-decorated polymeric micelles which can target folate receptor over-expressing tumor cells. Fluorescently labeled polymeric micelles were prepared using a lissamine-platinum complex linked in a similar manner as dactolisib. Dactolisib polymeric micelles showed good colloidal stability in water and released the coupled drug in buffers containing chloride or glutathione. Folate decorated micelles were avidly internalized by folate-receptor-positive KB cells and displayed targeted cellular cytotoxicity at 50–75 nM IC_{50}. In conclusion, we have prepared a novel type of folate-receptor targeted polymeric micelles in which platinum(II) linker chemistry modulates drug retention and sustained release of the coupled inhibitor dactolisib.

1. Introduction

Polymeric micelles are self-assembling nanoparticles that have gained increasing attention as nanocarriers for tumor delivery of cytostatic agents (Cabral and Kataoka, 2014; Cabral et al., 2018; Chao et al., 2012; Houdaihed et al., 2017; Varela-Moreira et al., 2017). Polymeric micelles have a core–shell structure consisting of a hydrophobic core that can accommodate hydrophobic drugs and an outer shell comprised of hydrophilic polymers which help in avoiding recognition by macrophages and prolonging circulation in the bloodstream. The small size of polymeric micelles enables them to accumulate in tumors via the enhanced permeability and retention (EPR) effect (Fang et al., 2011; Maeda et al., 2000). Moreover, when the nanocarrier surface is decorated with targeting ligands against tumor-cell-specific receptors, receptor-mediated endocytosis can selectively deliver the loaded drugs into tumor cells (Chen et al., 2015; Makino et al., 2015; Miura et al., 2013; Srinivasarao and Low, 2017; van der Meel et al., 2013; Wang et al., 2016). Importantly, this uptake pathway may overcome mechanisms of drug resistance and therefore enhance the efficiency of nanomedicines as compared to conventional small molecule drugs (Chen et al., 2017; Gothwal et al., 2016).

As mentioned, hydrophobic drugs can be loaded in the hydrophobic core of polymeric micelles. However, it has been reported that drug-loaded micelles have low stability in biological media and dissociate upon systemic administration, due to dilution below the critical micelle concentration and/or extraction of the drug by plasma proteins such as serum-albumin and lipoproteins (Chen et al., 2008; Shi et al., 2017; Sungwon et al., 2010). Two common strategies to improve the stability of drug-loaded polymeric micelles are crosslinking of the polymer core (Talelli et al., 2015) and conjugation of the drug to the core of micelles (Alani et al., 2010; Bae et al., 2003; Hu et al., 2015).

The coupling of drugs to the core of the micelles requires suitable linkers that on the one hand increase the extracellular stability of the micellar conjugates and on the other hand ensure the intracellular release of the drug. Commonly used linkers for bio-reversible coupling of drugs are pH responsive linkers (hydrazone and ester bonds) (Talelli et al., 2010; Ulbrich et al., 2004) and redox responsive linkers (disulfide) (Brülisauer et al., 2014; Meng et al., 2009; Yuan et al., 2017). A

* Corresponding author at: Department of Pharmaceutics, Utrecht Institute for Pharmaceutical Sciences, Utrecht University, Universiteitsweg 99, 3584 CG Utrecht, The Netherlands.
E-mail address: r.j.kok@uu.nl (R.J. Kok).

https://doi.org/10.1016/j.ijpharm.2020.119305
Received 10 January 2020; Received in revised form 2 April 2020; Accepted 3 April 2020
Available online 08 April 2020
0378-5173/

relative novel alternative are bioinorganic linker systems, such as the platinum(II) linker dichloro(ethylenediamine)platinum(II) (hereafter referred to as Lx linker) which has been used for synthesis of drug-protein and drug-polymer conjugates (Buwalda et al., 2019; Dolman et al., 2012; Dolman et al., 2008; Dolman et al., 2010; Harmsen et al., 2011; Prakash et al., 2008; van Dijk et al., 2019). Platinum coordination chemistry has several features that make it different from other linking approaches. Firstly, this type of linker reacts with aromatic nitrogen atoms and can consequently create conjugates with drugs that lack functionalities normally used for conjugation reactions (e.g. hydrazone, ester, disulfide based strategies). Secondly, platinum coordination bonds display relative high stability in biological media as compared to complexes with other transition metals such as for instance Ni(II) (Basolo, 1996; Reedijk, 2008). Platinum(II)-drug conjugates dissociate slowly even in biological media which is among others dependent on competitive displacement by electron-donating ligands such as glutathione (GSH) (Fretz et al., 2008; Sijbrandi et al., 2017).

In the present study, we coupled the hydrophobic kinase inhibitor dactolisib (DLB) via the platinum linker Lx to pendant carboxylic groups of poly(ethylene glycol)-*b*-poly(acrylic acid) (PEG-PAA) block copolymers; the formed polymer-Lx-drug complexes spontaneously self-assemble into polymeric micelles in an aqueous milieu due to hydrophobicity of the drug-modified PAA block (Shi et al., 2019b). DLB is a potent inhibitor of phosphatidylinositol-3-kinase (PI3K) and mammalian Target of Rapamycin (mTOR) and has been investigated as anticancer agent in phase II clinical trials. DLB has two aromatic nitrogen sites and its complexation with Lx hence can produce two linker-drug regio-isomers (Fig. 1A). Lx-DLBq is the conjugate of Lx coordinating to the quinoline ring of DLB while Lx-DLBiq is the conjugate of Lx coordinating to the imidazoquinoline ring of DLB. We isolated both Lx-DLB regio-isomers by preparative HPLC chromatography and prepared folate decorated polymeric micelles with either Lx-DLB regio-isomer (Fig. 1B–C).

In the present manuscript we report on the synthesis of platinum-linked DLB polymeric micelles and their physicochemical properties such as micellar stability and drug release kinetics. We further equipped the micelles with folate ligands by attachment of a sulfhydryl folate derivate to the distal end of the PEG corona. The folate receptor (FR) is a 38 kDa glycosyl-phosphatidylinositol (GPI) membrane anchored glycoprotein that is overexpressed in many human cancer cells, including ovarian and breast cancer cells (Leamon and Reddy, 2004). Folate (FA) binds to the FR with high affinity and is subsequently internalized by receptor-mediated endocytosis (Philip Stewart and Sumith Anurasiri, 2009). Numerous studies report on soluble drug-folate conjugates and (Shi et al., 2019a; Vlahov and Leamon, 2012) and folate decorated nanoparticles for selectively targeting tumors (Chen et al., 2017; Krzysztoń et al., 2017; van Dam et al., 2011). By investigating binding, uptake and cellular activity in FR-expressing and FR-negative cells, we have investigated the importance of active targeting (i.e. receptor mediated endocytosis and subsequent cellular processing) in the cellular activity of DLB loaded micelles.

2. Materials and methods

2.1. Materials

O-(2-aminoethyl)-*O'*-[2-(Boc-amino)ethyl]polyethylene glycol (M_n: 5,000 g/mol) (Boc-PEG-NH_2), 2-(dodecylthiocarbonothioylthio)-2-methylpropionic acid *N*-hydroxysuccinimide ester (CTA-NHS), *tert*-butyl acrylate (*t*BA), 2,2-azobis(2-methylpropionitrile) (AIBN), lauroyl peroxide (LPO), trifluoroacetic acid (TFA), 3-maleimidopropionic acid N-hydroxysuccinimide ester (Mal-NHS), *N*-(propionyloxy)succinimide (Prop-NHS), dichloro(ethylenediamine) platinum(II) [$PtCl_2$(en)] (Lx), lissamine™ rhodamine B sulfonylchloride, silver nitrate ($AgNO_3$), potassium thiocyanate (KSCN), lithium chloride, L-glutathione (GSH), DL-dithiothreitol (DTT), deuterated dimethyl sulphoxide (DMSO-d_6), methanol-d_4 (CD_3OD), tris base, sodium chloride, Tween 80, sodium hydroxide, bovine serum albumin (BSA) and formic acid were purchased from Sigma-Aldrich (Zwijndrecht, the Netherlands). Dactolisib (DLB) was purchased from LC Laboratories (Woburn, USA). Dimethylformamide (DMF), diethyl ether and acetonitrile were purchased from Biosolve BV (Valkenswaard, the Netherlands). 2,4,6-trinitrobenzene sulfonic acid (TNBSA) and micro bicinchoninic acid (BCA) protein assay kits were purchased from Pierce (Etten-Leur, the Netherlands). Poly(ethylene glycols) (PEGs) for GPC calibration were purchased from PSS Polymer Standards Services GmbH (Mainz, Germany). Phosphate buffered saline (PBS) pH 7.4 (8.2 g of NaCl, 3.1 g of Na_2HPO_4 dodecahydrate, 0.3 g of NaH_2PO_4 dihydrate per 1.0 L) was ordered from B. Braun Melsungen AG, Germany. Folate receptor alpha antibody (PA5-24186) and donkey anti-rabbit IgG (H + L) Alexa Fluor 488 secondary antibody (A-21206), Hoechst 33,42 solution (20 mM), radio-immunoprecipitation assay (RIPA) buffer, protease and phosphatase inhibitors were products of Thermofisher (Bleiswijk, the Netherlands). (3-(4,5-Dimethylthiazol-2-yl)-5-(3-carboxymethoxyphenyl)-2-(4-sulfophenyl)-2H-tetrazolium, inner salt) (MTS) cell proliferation assay kit was purchased from Abcam (Cambridge, UK). Phospho-Akt (Ser473) rabbit mAb, phospho-S6 ribosomal protein (Ser240/244) rabbit antibody, goat anti-rabbit horseradish peroxidase (HRP) conjugated secondary antibody and β-Actin rabbit mAb were purchased from Cell Signaling Technology (Leiden, the Netherlands). All other cell culture related materials were obtained from Gibco (Grand Island, NY, USA).

2.2. Synthesis and characterization of Lx-DLBq and Lx-DLBiq

Lx-DLBq and Lx-DLBiq were synthesized and purified as described before (Shi et al., 2019a). Optimal reaction conditions were determined by reaction DLB and Lx at different stoichiometric ratios. Briefly, cis-[Pt (ethylenediamine) nitrate chloride] was synthesized by reacting dichloro(ethylenediamine)platinum(II) [$PtCl_2$(en)] (Lx) (750 mg, 2.307 mmol) with $AgNO_3$ (390 mg, 1 eq) in 15 ml DMF overnight in the dark at room temperature (Prakash et al., 2008). The formed silver chloride precipitate was removed by filtration over a PTFE filter (0.2 μm cutoff, 47 mm diameter, Whatman). Subsequently, activated Lx was reacted with DLB at four different molar ratios: 1:1, 2:1, 3:1 and 4:1. DLB (400 mg, 0.85 mmol) was dissolved in 40 ml DMF and 1, 2, 3 and 4 equivalents activated Lx (0.69, 1.38, 2.08 and 2.77 ml) were respectively added to 5 ml DLB solution and reacted at 60 °C for 24 h. Next, 5 μl samples were taken and diluted with 195 μl DMF/H_2O 1:2 (v/v) and subsequently analyzed using UPLC and LC-MS as described in the supplementary material (Section 1.1; Fig. S1 and Table S1).

Next, a Waters preparative HPLC system was used to purify the synthesized Lx-DLBq and Lx-DLBiq present in the reaction mixture of DLB and activated Lx at 1:1 M feed ratio. The fractions that contained the aimed products (UPLC and LC-MS analysis) were pooled and freeze-dried. ^{1}H NMR spectroscopic analysis was used to identify which aromatic nitrogen atom of DLB was coordinated to the platinum linker Lx for Lx-DLBq and Lx-DLBiq, respectively (supplementary material Section 1.1; Fig. S2).

2.3. Synthesis and characterization of PEG-PAA copolymers

A reaction scheme of the synthesized polymers has been included in the supplementary information (Fig. S3).

2.3.1. Synthesis of Boc-PEG-CTA

2-(Dodecylthiocarbonothioylthio)-2-methylpropionic acid *N*-hydroxysuccinimide ester (CTA-NHS, 230.9 mg, 0.5 mmol) was dissolved in 5 ml DMSO and 139 μl of triethylamine (TEA, 1.0 mmol) was subsequently added. Next, a solution of *O*-(2-aminoethyl)-*O'*-[2-(Boc-amino) ethyl]polyethylene glycol (Boc-PEG-NH_2) (500.0 mg, 0.1 mmol) in 5 ml DMSO was slowly added to this reaction mixture (Chen et al., 2017;

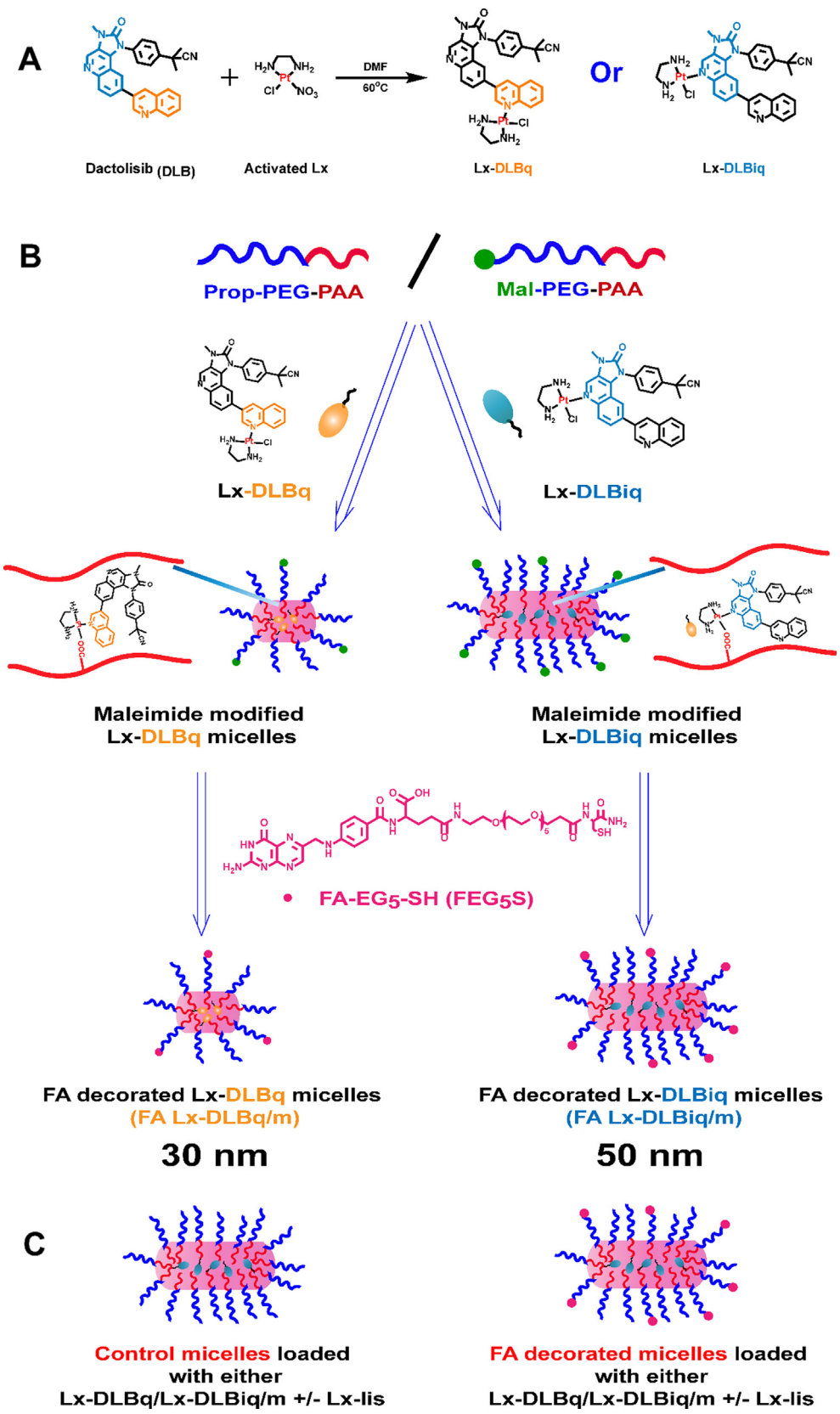

Fig. 1. Design and synthesis of folate decorated platinum-linked dactolisib polymeric micelles. (A) Two types of Lx-DLB regioisomers were synthesized: Lx-DLBq (linker conjugated to quinoline ring) and Lx-DLBiq (linker conjugated to imidazoquinoline ring). (B). Conjugation of either Lx-DLBq or Lx-DLBiq to PEG-PAA polymers induces self-assembly of drug-polymer unimers into polymeric micelles. Folate decorated micelles are prepared by reaction of the thiolated FA-derivative FA-EG_5-SH to maleimidyl-PEG groups at the surface of polymeric micelles. (C) Schematic depiction of FA-decorated and non-FA decorated micelles (control micelles) loaded with platinum-linked DLB and lissamine complexes.

Novo et al., 2014; Zhang et al., 2015). The reaction was allowed to proceed for 48 h under a nitrogen atmosphere in the dark. The product was purified by precipitation in 500 ml cold diethyl ether. The precipitated polymer was redissolved in 2 ml methanol and precipitated in 100 ml cold diethyl ether again. This dissolution/precipitation procedure was repeated three times. Subsequently, Boc-PEG-CTA was dried under vacuum at room temperature for 24 h and collected as yellow powder. The obtained polymer was characterized using GPC and ^{1}H NMR.

2.3.2. Synthesis of Boc-PEG-PtBA

Reversible addition fragmentation chain transfer (RAFT) polymerization (Fairbanks et al., 2015) was used to synthesize Boc-PEG-P*t*BA block polymers using Boc-PEG-CTA as a chain transfer agent, 2,2-azobis(2-methylpropionitrile) (AIBN) as a radical initiator and *tert*-butyl acrylate (*t*BA) as monomer (Germack and Wooley, 2010; Zhang et al., 2009). The polymerization procedure was the following: 400 mg of Boc-PEG-CTA (8.78×10^{-2} mol L^{-1}), 2.4 mg of AIBN (1.75×10^{-2} mol L^{-1}) and 398.8 mg of *t*BA (3.69 mol L^{-1}) were dissolved in 843 µl DMF and transferred into a 15 ml glass vial which was equipped with a magnetic stir bar. The molar feed ratio of *t*BA: Boc-PEG-CTA: AIBN was 42:1:0.2. Subsequently, the vial was capped with a rubber septum and the mixture was degassed by three freeze–pumpthaw cycles (liquid N_2-high vacuum-room temperature). After the final thaw cycle, the vial was backfilled with nitrogen, sealed and immersed in an oil bath thermostated at 80 °C to react for 4 h under a nitrogen atmosphere. Small aliquots (ca. 100 µl) were collected at 0 h and 4 h to determine the % *t*BA conversion using NMR analysis. The vial was then rapidly immersed in liquid nitrogen to quench the polymerization. The frozen mixture was thawed at room temperature and the formed polymer was precipitated into cold diethyl ether. Subsequently, the obtained Boc-PEG-P*t*BA-CTA was dried in vacuo overnight at room temperature and collected as yellow powder. The obtained Boc-PEG-P*t*BA-CTA was characterized using GPC, ^{1}H NMR and UV analysis. Next, the thiocarbonylthio end group of the polymer was removed using a radical induced reduction procedure (Chen et al., 2009; Chong et al., 2010). Typically, Boc-PEG-P*t*BA-CTA (600 mg, 0.063 mmol), AIBN (207 mg, 1.26 mmol) and lauroyl peroxide (LPO) (50.3 mg, 0.126 mmol) were dissolved in DMF (5 ml). This solution was degassed via three cycles of freeze–pumpthaw and heated at 80 °C to react for 4 h. Subsequently, the solution was cooled and the formed polymer was precipitated in 250 ml cold diethyl ether, collected by centrifugation and dried under vacuum for 24 h. The obtained polymer was characterized using GPC, ^{1}H NMR and UV analysis.

2.3.3. Deprotection of Boc-PEG-PtBA to yield NH_2-PEG-PAA

The conversion of Boc-PEG-P*t*BA into NH_2-PEG-PAA was done as follows. A glass vial (15 ml) with a magnetic stir bar was charged with Boc-PEG-P*t*BA (synthesized as described in Section 2.3.2, 500 mg, 0.053 mmol, corresponding to 1.684 mmol *tert*-butyl acrylate units) followed by the addition of dichloromethane (DCM, 3.86 ml). The resulting mixture was stirred for 5 min to dissolve the polymer and subsequently trifluoroacetic acid (TFA; 3.86 ml, 50.5 mmol) was added (Greene et al., 2011; Novo et al., 2014). The mixture was stirred at room temperature for 24 h and subsequently DCM and TFA were removed under reduced pressure. Next, the product was redissolved in 2 ml methanol and precipitated in 100 ml cold diethyl ether. This dissolution/precipitation procedure was repeated three times and the precipitated product was collected by centrifugation and dried under vacuum for 24 h. The obtained polymer was characterized using GPC, ^{1}H NMR and 2,4,6-trinitrobenzene sulfonic acid (TNBSA) analysis (Novo et al., 2014).

2.3.4. Synthesis of Mal-PEG-PAA and Prop-PEG-PAA

NH_2-PEG-PAA (300 mg, 0.038 mmol) was dissolved in 4.0 ml DMSO and divided into two aliquots. Next, 2 ml of 3-maleimidopropionic acid N-hydroxysuccinimide ester (Mal-NHS) (25.9 mg, 0.097 mmol) or 2 ml of *N*-(propionyloxy) succinimide (propionyl-NHS; prop-NHS) (16.7 mg, 0.097 mmol) DMSO solution mixed with 27 µl of triethylamine (TEA, 0.194 mmol) were added. The two reaction mixtures were subsequently stirred at room temperature for 48 h under a nitrogen atmosphere (Chen et al., 2017). The formed products, Mal-PEG-PAA (maleimide-PEG-PAA) and Prop-PEG-PAA (propionyl-PEG-PAA), were purified by dialysis against DMSO for 24 h, followed by a gradual exchange of the dialysis medium to deionized water. The products were obtained after freeze drying. The obtained polymers were characterized using GPC, ^{1}H NMR and TNBSA analysis (Supplementary information, Table S2 and Figs. S4–S8).

2.4. Preparation and characterization of micelles

2.4.1. Preparation of Lx-DLB loaded micelles

Lx-DLBq (19 mg) was dissolved in 10 ml distilled water for 20 min at 70 °C to obtain a concentration of 2.5 mM. Next, this solution was cooled to 37 °C and added dropwise to an Prop-PEG-PAA aqueous solution ([AA] = 5.0 mM; [Lx-DLBq]: [AA] = 1:2 mol/mol, pH was adjusted to 7.4 using 0.5 N NaOH, 10 ml) (Ahn et al., 2015). Once Lx-DLBq is coordinated to the pendant carboxylic groups of PAA, the block polymer becomes amphiphilic and consequently self-assembles into Lx-DLBq/m polymeric micelles composed of a PEG shell and PAA-Lx-DLBq core. After stirring for 16 h at 37 °C, the mixture was transferred into a Millipore stirred ultrafiltration cell equipped with an Amicon mini-reservoir RC800 and a concentration/dialysis selector valve model CDS10 (molecular weight cut-off size of 100 kDa). Lx-DLBiq loaded micelles (Lx-DLBiq/m) were prepared using the same procedures.

Folate decorated micelles were prepared by a similar procedure as described above, making use of thiol-maleimidyl coupling chemistry. A thiolated FA-penta-ethylen derivative (FA-EG_5-SH) was synthesized (supplementary information Fig S9), as described elsewhere (Shi et al., 2019a) and reacted to maleimidyl-PEG containing micelles. Lx-DLBq or Lx-DLBiq aqueous solutions were added dropwise to a solution of Mal-PEG-PAA and Prop-PEG-PAA ([AA] = 5.0 mM; [Lx-DLB]:[AA] = 1:2 mol/mol, [Mal-PEG-PAA]:[Prop-PEG-PAA] = 1:3 mol/mol). After purification by ultrafiltration, FA-EG_5-SH (FEG_5S) (0.68 mg, 0.0781 mmol, 2.0 eq. vs maleimide group) was added to the maleimide functionalized micellar dispersion (10.0 ml) and incubated at room temperature for 16 h. Finally, the micellar dispersion was purified by ultrafiltration (MWCO, 100,000) to yield folate decorated micelles loaded with Lx-DLBq (FA Lx-DLBq/m) or Lx-DLBiq (FA Lx-DLBiq/m). The volume of the micelle dispersion was adjusted by ultrafiltration with water to 5.0 ml and stored at 4 °C until further use. To confirm folate coupling, 2.0 ml FA Lx-DLBq/m micelle dispersion was lyophilized and the solid product was redissolved in D_2O to for ^{1}H NMR spectroscopic analysis (Fig. S10).

Fluorescently labeled micelles were prepared by coordinating a 4:1 mol:mol mixture of Lx-DLB and Lx-lissamine (Lx-lis, the synthesis and characterization of Lx-lissamine were described in supplementary information Section 1.2) to PEG-PAA copolymers, followed by the subsequent reaction and purification steps described above.

2.4.2. Characterization of micelles

The size and size distribution of the different micelles were determined by dynamic light scattering (DLS, Zetasizer Nano S, Malvern Instruments, UK) of 1 mg/ml micellar dispersions in water at 25 °C. The zeta potential (ζ) was measured of 1 mg/ml micellar dispersions in 20 mM HEPES (pH 7.4) using a Malvern Zetasizer Nano-Z (Malvern Instruments, UK) with universal ZEN 1002 'dip' cells and DTS (Nano) software (version 4.20) at 25 °C. The morphology of the micelles was visualized by Transmission Electron Microscope (TEM, JEM-1400, JEOL, Japan) operated with 100 kv acceleration voltages and 40 µA beam current. Micelles with a concentration of 1 mg/ml in water were stained with uranyl acetate solution (2%, w/v) and the samples were placed on 400-mesh copper grids for TEM measurement (Cabral et al., 2011). Static light scattering (SLS) of the micelles was measured on a Sofica goniometer using a He-He laser. Prior to the light scattering measurements, 1 mg/ml Lx-DLBq/m or Lx-DLBiq/m aqueous dispersions were filtered through Millipore Teflon (Nylon) filters with a pore size of 0.45 µm. R_g (the radius of gyration), R_h (the hydrodynamic radius), weight-average molecular weights (M_w) and N_{agg} (the aggregation number) were obtained from SLS measurements (Chu and Liu, 2000).

The DLB loading content of the micelles was determined after their

destruction by incubation with potassium thiocyanate (KSCN) which is a strong ligand for platinum(II) coordination (Harmsen et al., 2011). Lx-DLBq/m and Lx-DLBiq/m were separately dispersed at a concentration of 2.5 mg/ml in PBS containing 0.5 M KSCN and 1% v/v Tween 80 (added to solubilize the released hydrophobic drug) and incubated at 80 °C for 24 h. Next, samples were diluted with DMF to fall in the calibration range of DLB (0.125 to 40 μg/ml) and analyzed using UPLC as described in supplementary information Section 1.1.3. Drug loading capacity (LC) and loading efficiency (LE) were calculated using Eqs. (1) and (2).

$$LC = \frac{\text{weight of DLB measured}}{\text{weight of DLB loaded micelles}} \times 100\% \quad (1)$$

$$LE = \frac{\text{weight of DLB measured}}{\text{weight of DLB added}} \times 100\% \quad (2)$$

2.5. Stability of the micelles

The colloidal stability of the micelles was studied after incubation for 72 h at 37 °C in Milli Q H_2O and phosphate buffered saline (PBS) pH 7.4 (8.2 g of NaCl, 3.1 g of $Na_2HPO_4{\cdot}12H_2O$, 0.3 g of $NaH_2PO_4{\cdot}2H_2O$ per 1.0 L). Small sample aliquots were analyzed by DLS and changes in size and size distribution were compared with freshly prepared dispersions of the micelles (Uchino et al., 2005).

2.6. In vitro DLB release

The *in vitro* release of DLB from the micelles was evaluated using a dialysis method at 37 °C in four different media: (i) Milli Q H_2O containing 1% v/v Tween 80; (ii) PBS containing 1% v/v Tween 80; (iii) PBS containing 10 mM glutathione (GSH) and 1% v/v Tween 80; and (iv) PBS containing 10 mM dithiothreitol (DTT) and 1% v/v Tween 80 (Temming et al., 2006). Tween 80 was added to the media to solubilize the released DLB and thus maintain sink conditions. One ml Lx-DLBq/m or Lx-DLBiq/m micellar dispersions (corresponding to 2.35 mg/ml DLB) were transferred into dialysis tubes (Spectra-Por® Float-A-Lyzer® G2, MWCO 100 kDa) and immersed into 19 ml of the different release media (compositions given above). Samples were incubated at 37 °C under constant shaking. Five ml samples from the outer dialysis solution were withdrawn at 0, 3, 6, 9, 24, 48, 72 and 96 h and replenished with an equal volume of corresponding fresh medium. Each experiment was repeated three times. The concentration of released DLB in the different media was analyzed using UPLC as described in supplementary information Section 1.1.3.

2.7. Cell culture

KB cells (a FR-positive malignant human cancer cell line) and A549 cells (a FR-negative human lung carcinoma cell line) were obtained from the American Type Culture Collection (ATCC, Manassas, Virginia, USA) (Henne et al., 2013). KB cells were maintained in low glucose Dulbecco's modified Eagle's medium (DMEM) supplemented with 10% (v/v) fetal bovine serum (FBS) and A549 cells were maintained in DMEM/F12 culture medium also supplemented with 10% (v/v) FBS. The cells were cultured in a humidified atmosphere containing 5% CO_2 at 37 °C.

2.8. Immunostaining and detection of folate receptors

KB and A549 cells were seeded in a 24-well plate (4×10^4 cells/well) and incubated for 24 h in low glucose DMEM medium (for KB cells) and DMEM/F12 medium (for A549 cells) with 10% FBS. Subsequently, 20 μl Hoechst 33342 (1:1000 dilution in culture medium) was added to the wells and incubated for 30 min to stain the nuclei of the cells. After washing with PBS, the cells were fixed with 4% paraformaldehyde in PBS pH 7.4 for 10 min at room temperature. The cells were subsequently washed three times with ice-cold PBS and incubated with 1% bovine serum albumin (BSA) in PBST (PBS + 0.1% Tween 20) for 30 min to block unspecific binding of the antibodies. After washing with PBS, the cells were incubated with folate receptor alpha antibody (PA5-24186, dilution 1:20) in 1% BSA in PBST in a humidified chamber for 1 h at room temperature (Chen et al., 2017). After washing with PBS three times, the cells were incubated with donkey anti-rabbit IgG (H + L) Alexa Fluor 488 secondary antibody (A-21206, dilution 1:200) in 1% BSA for 1 h at room temperature in the dark. Next, the cells were washed with PBS three times and imaged using Keyence BZ-9000 microscopy fluorescent microscope. Digital images were acquired using two channels: a blue channel (λ_{ex} 405 nm, λ_{em} 445 nm) for nuclei, and green channel (λ_{ex} 488 nm, λ_{em} 525 nm) for folate receptor. The images were analyzed by ImageJ and the relative area fraction of folate receptor was calculated.

2.9. Cellular binding studies

KB cells (FR^+) and A549 cells (FR^-) were seeded into 96-well plates at density of 1.6×10^4 cells/well and 1.2×10^4 cells/well respectively. After incubation for 24 h at 37 °C, 200 μl medium was replaced with media containing micelles (final concentration was 10 μM lissamine) in culture medium. Then, the cells were incubated on ice for 30 min in the dark (Liu et al., 2017; van der Meel et al., 2012). For competition experiments with free folate, KB and A549 cells were pretreated with 1000 μM folate (i.e. 100-fold molar excess compared to folate coupled to the micelles) on ice for 30 min before addition of the micelles. Subsequently, 5 μl Hoechst 33342 (1:1000 dilution in PBS) was added into the wells and the cells were incubated on ice for 30 min to stain their nuclei. Thereafter, the cells were washed three times with cold PBS and fixed with 4% formalin for 10 min on ice. Next, the plates were transferred into a fully automated Yokogawa High Content Imaging Platform (Model CV7000, Yokogawa, Tokyo, Japan). Confocal images were acquired using a 60× oil objective at two channels: a channel (λ_{ex} 405 nm, λ_{em} 445 nm) for nuclei and another channel (λ_{ex} 488 nm, λ_{em} 600 nm) for lissamine. The mean lissamine fluorescence intensity was analyzed by ImageJ software. All experiments were performed in triplicate.

2.10. Internalization of micelles

Cellular internalization of Lx-DLBq&lis/m, FA Lx-DLBq&lis/m, Lx-DLBiq&lis/m and FA Lx-DLBiq&lis/m micelles was conducted as described for the cellular binding experiments (Section 2.9), with the following differences: (1) The incubations were done at 37 °C; (2) The incubation time of the micelles with the cells was 2 h; (3) PBS instead of cold PBS was used to wash the cells; (4) The cells were not fixed with 4% formalin before being transferred into the Yokogawa High Content Imaging Platform for confocal imaging.

2.11. Effects on mTOR and PI3K signaling cascades

Specific inhibitory activity of DLB and DLB loaded micelles was determined by phospho-western blot analysis of proteins downstream in the of PI3K/mTOR signaling pathway, phospho-Akt (Ser473) and phospho-S6 ribosomal protein (Ser240/244), respectively (Gholizadeh et al., 2018; Liu et al., 2009). Briefly, KB cells were seeded in 6 well plates at a density of 2×10^5 cells/well and allowed to adhere overnight. Subsequently, 80 nM free DLB, 80 nM Lx-DLBq/m, 80 nM FA Lx-DLBq/m, 80 nM FA Lx-DLBq/m + 8 μM folate (100-fold excess), 80 nM Lx-DLBiq/m, 80 nM FA Lx-DLBiq/m, 80 nM FA Lx-DLBiq/m + 8 μM folate (100-fold excess compared to folate modified on the micelles) and 8 μM folate were added to the cells. The cells were incubated for 16 h at 37 °C, followed by washing with cold PBS and subsequently the cells were lysed with radio-immunoprecipitation assay buffer (RIPA),

supplemented with phosphatase/kinase inhibitor cocktail (Thermofisher, Bleiswijk, the Netherlands) for 30 min on ice (Gholizadeh et al., 2018). The resulting cell lysates were centrifuged at 12,000*g* for 15 min and the protein concentration in the supernatants was quantified using the Pierce™ bicinchoninic acid (BCA) protein assay kit. The supernatants were also subjected to SDS-PAGE analysis using 4–12% gradient NuPAGE Novex Bis-Tris mini-gels (Invitrogen, Breda, the Netherlands). Proteins were electro-transferred onto a nitrocellulose membrane via iBlot Dry Blotting system. After blocking with 5% BSA in Tris-Buffered Saline containing 0.1% Tween-20 (TBS-T) for 1 h at room temperature, the membranes were incubated with primary antibodiesphospho-S6 ribosomal protein (Ser240/244) rabbit mAb, phospho-Akt (Ser473) rabbit mAb and β-Actin rabbit mAb for 16 h at 4 °C. After washing with TBS-T for three times, the membranes were incubated with goat anti-rabbit horseradish peroxidase (HRP) conjugated secondary antibody at room temperature for 2 h. After three washings with TBST buffer, protein expression was visualized by using the enhanced chemiluminescence (ECL) western blotting reagent and the membranes were scanned with a Gel Doc Imaging system equipped with one XRS camera.

2.12. Effects of DLB loaded micelles on cell viability

The cytotoxicity of DLB, Lx-DLBq/m, FA Lx-DLBq/m, Lx-DLBiq/m and FA Lx-DLBiq/m against KB and A549 cell lines was evaluated using the (3-(4,5-dimethylthiazol-2-yl)-5-(3-carboxymethoxyphenyl)-2-(4-sulfophenyl)-2H-tetrazolium, inner salt) (MTS) cell proliferation assay kit. In short, KB cells (FR^+) and A549 cells (FR^-) were seeded into 96-well plates at a density of 5×10^3 cells/well, respectively, and incubated for 24 h at 37 °C in a culture medium containing 10% FBS. The cells were then incubated with DLB, Lx-DLBq/m, FA Lx-DLBq/m, Lx-DLBiq/m and FA Lx-DLBiq/m at concentrations of 10–5120 nM equivalent DLB for 72 h under 5% CO_2 at 37 °C (Wu et al., 2014). Subsequently, 40 μl MTS reagent was added to the wells and the MTS assay was performed according to manufacturer's protocol. The absorbance at 492 nm was measured using a microplate reader (Thermoscientific Multiskan MK3). The cytotoxicity is expressed as the percentage of viable cells compared to untreated control cells. For competition cytotoxicity experiments with free folate, KB cells were exposed to 320 nM (equivalent DLB) Lx-DLBq/m, FA Lx-DLBq/m, Lx-DLBiq/m and FA Lx-DLBiq/m with or without 32 μM folate (100-fold excess) and A549 cells were exposed to 5120 nM (equivalent DLB) Lx-DLBq/m, FA Lx-DLBq/m, Lx-DLBiq/m and FA Lx-DLBiq/m micelles with/without 512 μM folate (100-fold excess). Next, the cells were incubated at 37 °C for 72 h after which the cell viability was measured by the MTS assay in the similar way as described above.

2.13. Statistical analysis

Unless otherwise mentioned, triplicate data were obtained and presented as mean ± standard deviation. GraphPad Prism software version 7 (GraphPad Software, Inc.) was used for statistical analysis performed by two-way analysis of variance (ANOVA) and significance differences were considered when P value < 0.05.

3. Results and discussion

3.1. Synthesis and characterization of Lx-DLBq and Lx-DLBiq

Dactolisib has two aromatic nitrogen groups (in quinoline ring and imidazoquinoline, respectively) which can coordinate with the Lx linker to form platinum-coordination complexes (Fig. 1). Both Lx-DLB regio-isomers were isolated by preparative HPLC with a yield of 16% and 21% versus the starting amount of DLB. UPLC chromatograms of the purified compounds are shown in Fig. 2, demonstrating that Lx-DLB complexes had a high purity (> 95%). Lx-DLB regio-isomers eluted earlier than starting compound DLB indicating that coupling of Lx to DLB had increased the hydrophilicity of the compounds, which can be attributed to the positive charge of the platinum(II) coordination complexes. We also observed good aqueous solubility of Lx-DLB regio-isomers while DLB is only marginally soluble in water (log P = 5.2) (Gholizadeh et al., 2018). Fig. 2B, D, F show the ^{1}H NMR spectra of DLB, and the purified Lx-DLB complexes. By comparing the ^{1}H NMR spectra of Lx-DLB (Fig. 2D) and DLB (Fig. 2B), it can be seen that the proton labeled "2" (8.77 ppm; d, J = 2.3 Hz, 1H) has shifted to 9.58 ppm (d, J = 2.1 Hz, 2H) while the proton labeled "1" shifted from 9.04 ppm to 9.12 ppm. This result demonstrates that the linker is coordinated to the aromatic nitrogen atom of the quinoline ring and we hence named this compound Lx-DLBq (Lx-DLB quinoline isomer). By comparing the ^{1}H NMR spectra of the other Lx-DLB isomer (Fig. 2F) and DLB, it can be seen that the proton labeled "1" (9.04 ppm (s, 1H)) has shifted to 9.54 ppm (s, 1H) while the proton labeled "2" had not shifted (Fig. 2F). This result demonstrates that the linker is coordinated to the aromatic nitrogen atom of the imidazoquinoline ring and we further named the regio-isomer Lx-DLBiq (Lx-DLB imidazoquinoline isomer).

3.2. Synthesis and characterization of PEG-PAA copolymers

The synthesis and characterization of PEG-PAA block copolymers Boc-PEG-CTA, Boc-PEG-P*t*BA, NH_2-PEG-PAA, propionyl-PEG-PAA (Prop-PEG-PAA) and maleimide-PEG-PAA (Mal-PEG-PAA) have been included in the supplementary information (Section 2.3). The final polymers that were used for preparation of micelles were Prop-PEG-PAA and Mal-PEG-PAA with number average molecular weights of $7.5 * 10^3$ g/mol (M_n, determined by NMR, Fig. S7). The size of the block lengths was $5.3 * 10^3$ g/mol for the PEG block and $2.2 * 10^3$ g/mol for the PAA block (corresponding to 30 acrylate units). Further polymer characteristics are listed in the supplementary Table S2.

3.3. Preparation and characterization of micelles

Lx-DLB was conjugated to PEG-PAA polymers at [Lx-DLB]:[AA] = 1:2 M ratio. The conjugation of positively charged Lx-DLB to the water soluble polymers eventually neutralized the negative charge of the PAA domain and, moreover, created a hydrophilic-hydrophobic block drug-copolymer conjugates which self-assembled into polymeric micelles with a densely packed core (Fig. 3). The DLB loading capacity (LC) of the micelles was determined by disruption of the drug-platinum (II) coordination bond by adding an excess of a platinophilic ligand, thiocyanate (SCN^-) and incubation for 24 h at 80 °C. The LC of Lx-DLBq/m was 18% while that of Lx-DLBiq/m was 20%, corresponding to 48–55% drug loading efficiencies (LE, Table 1). Although platinum(II) prefers amine and sulfhydryl groups over carboxylates for coordinative complexation, carboxylate complexes of platinum(II) are relatively stable as observed for polymeric micelles with the anticancer drugs carboplatin and cisplatin (Cabral et al., 2005; Nishiyama et al., 2001).

The morphology and size of the formed micelles were studied by DLS, SLS and TEM. As determined by DLS, the hydrodynamic diameter of the micelles prepared with Lx-DLBq was around 30 nm while that of the micelles prepared with Lx-DLBiq was around 50 nm (Fig. 3A-B, Table 1). We studied the morphology of the micelles with TEM and observed slightly elongated rod-like particles for Lx-DLBiq loaded micelles but not for Lx-DLBq loaded micelles. The size of the micelles was also determined by SLS which technique yields the R_g (the radius of gyration), R_h (the hydrodynamic radius), shape factor ($\rho = R_g/R_h$), N_{agg} (the aggregation number) and the density of the micelles. As can be seen in Table 1, the hydrodynamic radius of both micelles determined by SLS is in agreement with the hydrodynamic radius of the micelles determined by DLS, which is based on the assumption that the particles are spherical. The shape factor ρ defined as R_g/R_h (determined by SLS) for both micelles was 2.3, indicating an asymmetrical rod-like shape. According to the literature, the ρ value is 0.778, 1.27–2.05 and > 2.2 for uniform spheres, random coils and rods, respectively (Chu and Liu,

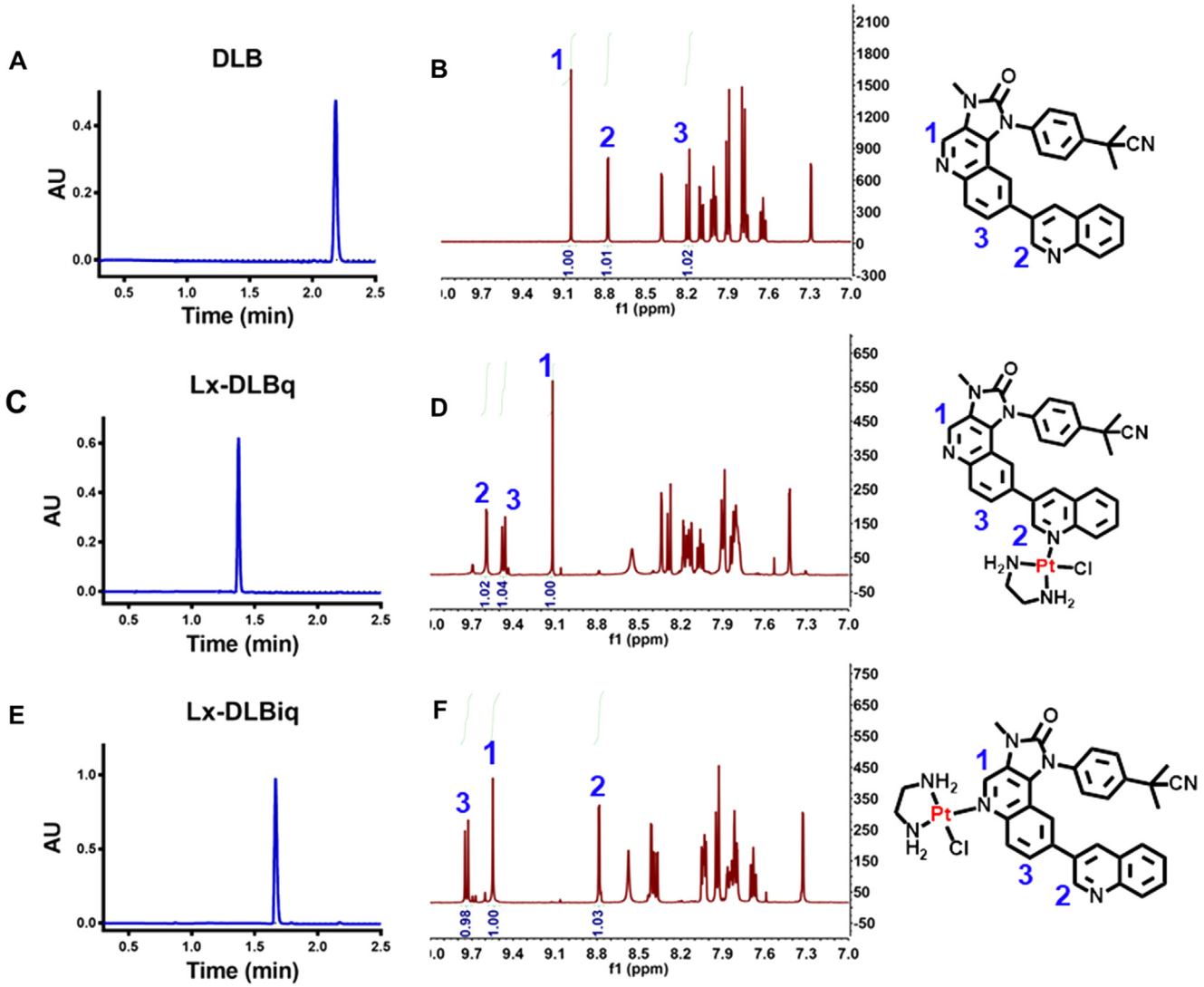

Fig. 2. (A, B) UPLC and NMR analysis of DLB. (C, D) UPLC and NMR analysis of purified Lx-DLBq. (E, F) UPLC and NMR analysis of purified Lx-DLBiq. Expansion of the ^{1}H NMR spectra in the 7–10 ppm region with the integrations of the peaks is shown. Full spectra (0–10 ppm) have been included in the supplementary information (Supplementary Fig. S2).

2000; Müller and Burchard, 1995). Lx-DLBiq micelles were larger as compared to the Lx-DLBq micelles and had an aggregation number (N_{agg}) of 733 vs 85, respectively. Possible explanations for the differences in size and shape between the two types of polymeric micelles may be differences in hydrophobicity of the drug-polymer conjugates, or differences in spatial orientation of the Lx-DLB regio-isomers. Lx-DLBiq is slightly more hydrophobic than Lx-DLBq, as can be deduced from their order of elution in reversed phase chromatography. A higher hydrophobicity may result in a more condensed packing of the core of the micelles, which also will affect the aggregation number. Differences in the spatial orientation of Lx-DLBiq versus Lx-DLBq may change the accessibility of the planar rings of DLB when attached to the PEG-PAA polymer, such for instance at the extended position of the free quinoline moiety. This may lead to improved stacking properties of the Lx-DLBiq-equipped polymer which may induce hydrophobic and π-π stacking interactions. We could not substantiate this hypothesis further, due to lack of time and resources. Linkage of DLB via the imidazoquinoline ring to the polymer backbone apparently afforded a better scaffold for polymer assembly resulting in larger Lx-DLBiq rod-like micelles.

We labeled DLB polymeric micelles by incorporation of a fluorescent dye (Lx-lissamine) which was conjugated to the PAA block in a similar manner as Lx-DLB. Folate decorated micelles were prepared by post-conjugating thiol-containing FA-EG$_5$-SH (FEG$_5$S) onto maleimide-functionalized Lx-DLB micelles prepared with a 1:3 mol:mol mixture of Mal-PEG-PAA and prop-PEG-PAA. Table 2 reports the size, PDI and zeta potential of the final six micellar products composed of different combinations of Lx-DLB regio-isomers, with and without Lx-lissamine and/or folate targeting ligand. The presence of folate ligand on the surface of FA Lx-DLBq/m micelles was confirmed by ^{1}H NMR spectroscopy of freeze-dried micelles dispersed in D$_2$O (Supplemental Fig. S10).

3.4. Micellar colloidal stability

Fig. 4A shows that both Lx-DLBq/m and Lx-DLBiq/m maintained their size and PDI upon incubation for 72 h in water at 37 °C, indicating that Lx-DLB micelles displayed high colloidal stability in this medium and at this temperature. In contrast, the size of Lx-DLBiq/m micelles increased from 50 to 67 nm (1.3-fold increase) whereas the size of FA Lx-DLBiq/m micelles increased from 54 to 65 nm (1.2-fold increase) upon incubation for 72 h in PBS at 37 °C (Fig. 4B). This increase in size was associated with an increase in PDI, from 0.10 to around 0.25. The increase in size coincided with release of Lx-DLB (but not free DLB) when the micelles were incubated in PBS buffer (containing 150 mM chloride ions) (Fig. 5C–D); Lx-DLB release was not observed after

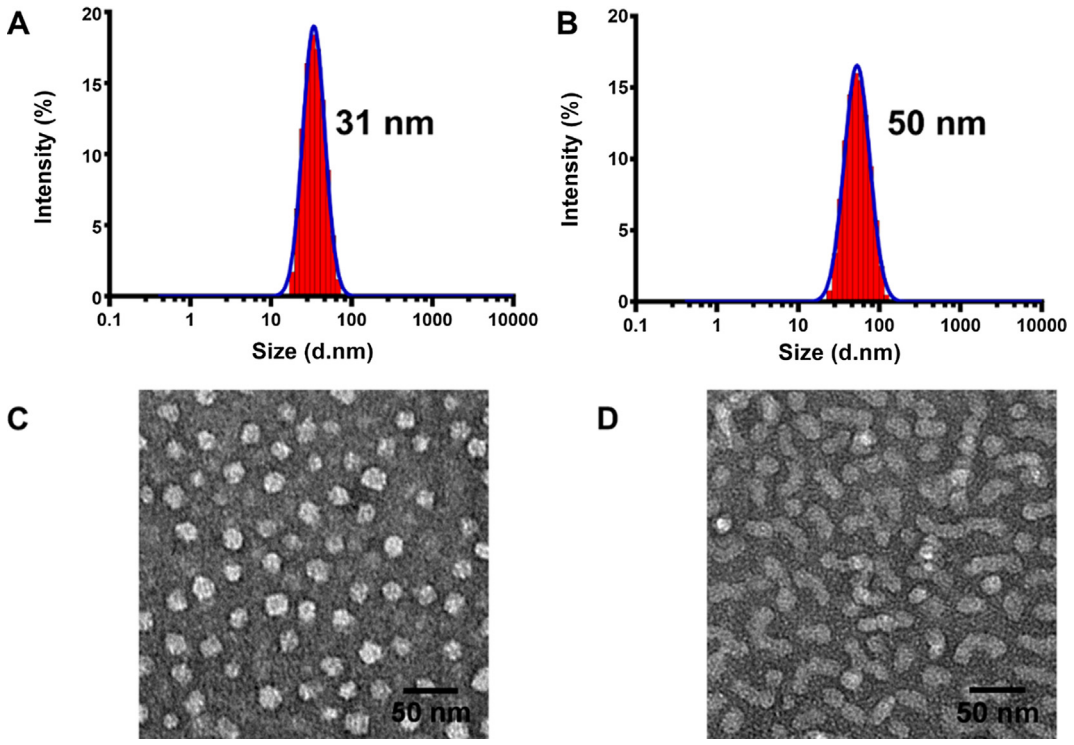

Fig. 3. (A) DLS histogram of Lx-DLBq micelles. (B) DLS histogram of Lx-DLBiq micelles. (C) TEM image of Lx-DLBq micelles, scale bar: 50 nm. (D) TEM image of Lx-DLBiq micelles, scale bar: 50 nm.

incubation in water (Fig. 5A–B). The release of Lx-DLB from the micelles in PBS will increase the hydrophilicity of the PAA-based core and thus its hydration, which explains the observed increases in size and PDI in PBS. The most likely mechanism for Lx-DLB release from micelles in PBS is chloride ion triggered disruption of platinum-carboxylate coordinative bonds (as schematically depicted in Fig. 5I). Chloride triggered drug release was also observed for cisplatin and DACHPt micelles developed by Kataoka and co-workers (Cabral et al., 2011; Nishiyama et al., 2001; Uchino et al., 2005). Upon intravenous administration, DACHPt-loaded micelles showed high stability in the blood circulation and extensive accumulation in C26 solid tumor (10% of the injected dose/g, versus 1% injected dose/g for oxaliplatin). Similar results were observed for cisplatin-loaded PEG-b-poly(L-glutamic acid). Thus, platin-drug loaded micelles have advanced into clinical trials with good tolerability and acceptable efficacy despite *in vitro* instability in presence of chloride containing buffers. The observed release of Lx-DLB from the micelles in PBS is slower as compared to cisplatin or DACHPt, which may relate to the more hydrophobic nature of the DLB.

3.5. Drug release

Fig. 5 shows the release of DLB from Lx-DLB polymeric micelles upon incubation in different media at 37 °C up to 4 days. All incubation media contained 1% v/v Tween 80 to solubilize the released DLB and Lx-DLB. As discussed above and shown in Fig. 5A–B, neither free DLB nor Lx-DLB were released from Lx-DLBq/m or Lx-DLBiq/m micelles in pure water. On the other hand, incubation in PBS resulted in around 30% Lx-DLB release but no release of free DLB (Fig. 5C–D). In media containing platinophilic ligands such as GSH and DTT, however, parent drug DLB was released with a cumulative release of approximately 20% in the presence of GSH and 30% in the presence of DTT upon incubation

Table 1
Characteristics of drug loaded polymeric micelles Lx-DLBq/m and Lx-DLBiq/m. Mean values with corresponding standard deviations are shown (n = 3).

Sample	DLS Size (d.nm)[a]	DLS PDI[b]	Zeta Potential (mV)	SLS R_g (nm)[c]	SLS R_h (nm)[d]	ρ[e] (R_g/R_h)	SLS N_{agg}[f]	TEM Size (d.nm)[g]	LC%[h]	LE%[i]
Micelles with quinoline linked DLB Lx-DLBq/m	31 ± 0	0.10 ± 0.02	−7.5 ± 0.9	38	17	2.3	85	19 ± 3	17.4 ± 0.6	46.0 ± 1.5
Micelles with imidazoquinoline linked DLB Lx-DLBiq/m	50 ± 1	0.12 ± 0.03	−6.0 ± 0.4	60	26	2.3	733	38 ± 4	21.0 ± 0.4	55.3 ± 1.2

[a] Hydrodynamic diameter size as determined by DLS.
[b] PDI: polydispersity index, determined by DLS.
[c] R_g is the radius of gyration as determined by SLS.
[d] R_h is the hydrodynamic radius as determined by SLS.
[e] ρ is shape factor which is equal to R_g/R_h.
[f] N_{agg} is the polymer-linker-drug aggregation number determined by SLS and calculated by dividing the weight-averaged M_w of particles ($1.5 * 10^6$ g/mol and $9.0 * 10^6$ g/mol for Lx-DLBq micelles and Lx-DLBiq micelles, respectively, determined by SLS) by the molecular weight of polymer-linker-drug.
[g] Diameter size as determined by TEM.
[h] LC: loading capacity, determined using UPLC.
[i] LE: loading efficiency, determined by UPLC.

Table 2
Characteristics of Lx-DLB loaded micelles with and without folate/lissamine. Mean values with corresponding standard deviations are shown (n = 3).

No.	Sample	Size (nm)[a]	PDI[b]	Zeta Potential (mV)
1	Folate decorated micelles FA Lx-DLBq/m	33 ± 2	0.11 ± 0.01	−9.0 ± 0.3
2	Fluorescently labeled control micelles Lx-DLBq&lis/m	30 ± 1	0.12 ± 0.01	−7.7 ± 1.0
3	Fluorescently labeled folate decorated micelles FA Lx-DLBq&lis/m	34 ± 0	0.15 ± 0.00	−9.4 ± 0.4
4	Folate decorated micelles FA Lx-DLBiq/m	56 ± 2	0.13 ± 0.02	−8.2 ± 0.6
5	Fluorescently labeled control micelles Lx-DLBiq&lis/m	47 ± 1	0.13 ± 0.00	−7.7 ± 1.0
6	Fluorescently labeled folate decorated micelles FA Lx-DLBiq&lis/m	54 ± 1	0.14 ± 0.01	−9.1 ± 0.1

[a] Diameter size determined by DLS.
[b] PDI: polydispersity index, determined by DLS

for 96 h at 37 °C (Fig. 5E–H). Relative rations of DLB release and Lx-DLB release changed depending on the platinophilic agent with highest amounts of free DLB for DTT. DTT has two thiol groups versus a single thiol for GSH, which makes DTT a stronger reducing and platinophilic agent, although GSH driven release probably better reflects intracellular conditions. The total amount of release of DLB (i.e. DLB + Lx-DLB) was similar for GSH and DTT containing media (Fig. 5E–H, blue curves, 65–70% DLB remaining in micelles after 96 h). Noteworthy, the intracellular concentration of glutathione (GSH) is approximately 0.5–10 mM while its extracellular concentration is approximately 0.01 mM (Li et al., 2015; Meng et al., 2009). As such, it seems likely that conversion of Lx-DLB into DLB mainly occurs after internalization of either micelles or Lx-DLB that is released extracellularly from micelles before their internalization.

3.6. Immunostaining and detection of folate receptors

The expression of folate receptor was investigated by immunofluorescent staining with an anti-folate receptor antibody (Fig. 6). KB cells showed strong staining indicative of the presence of the folate receptor at the cellular membrane, whereas hardly any staining could be detected for folate receptor-negative A549 cells (Fig. 6A and B). These results are in agreement with previous publications (Péraudeau et al., 2018; Yang et al., 2011).

3.7. Cellular binding and internalization of micelles

The cellular binding and internalization of fluorescently labeled micelles by KB and A549 cells was studied using confocal microscopy. Fig. 7 shows the confocal images and their semi-quantitative analysis upon incubation of the cells with micelles for 1 h at 4 °C. As expected, control Lx-DLB polymeric micelles without folate decoration did not bind to either cell type. In contrast, folate decorated micelles displayed distinctive binding on the cell membrane of KB cells -which are FR positive- but not A549 cells. Importantly, cellular binding of folate decorated micelles to KB cells was significantly inhibited by excess free folate which demonstrates that the binding was mediated by folate-receptor. The corresponding mean fluorescence intensity (MFI) is shown in Fig. 7B. Taken together, the results of Figs. 6 and 7 demonstrate that FA decorated micelles interact with FR expressing cells, while control micelles do not associate with cells.

Internalization of micelles was investigated by incubation of cells with micelles at 37 °C for 2 h, and yielded images of KB cells in which lissamine-related fluorescence had accumulated in a punctuated pattern, indicative of receptor-mediated uptake and lysosomal routing of folate decorated micelles but not control micelles (Fig. 8). Incubation with excess free folate abolished the internalization largely. Fig. 8B shows the semiquantitative comparison of uptake between the different micelles and cell types. Relative fluorescence signals of cells incubated with excess free folate were similar to the signal of control micelles without FA targeting ligand or uptake in A549 cells. Taken together, these results suggest that FA-decorated micelles are internalized via FR mediated internalization, which involves clustering of folate receptors due to the multivalent interaction of folate-decorated micelles with the cells (Davis et al., 2008; Jones et al., 2016).

3.8. Cellular effects of DLB loaded polymeric micelles

Pharmacological activity of DLB upon incubation of KB cells with polymeric micelles was investigated by Western blotting of phosphorylated S6 ribosomal protein and phosphorylated Akt, two downstream targets of the kinases inhibited by DLB. Fig. 9 shows the Western blot of KB cells that had been incubated with 80 nM DLB or polymeric micelles dispersions equivalent to 80 nM DLB for 16 h at 37 °C. Both free DLB and folate targeted micelles (FA Lx-DLBq/m and FA Lx-DLBiq/m) inhibited phosphorylation of the S6 ribosomal subunit strongly, while phosphorylation of Akt kinase had decreased less prominently.

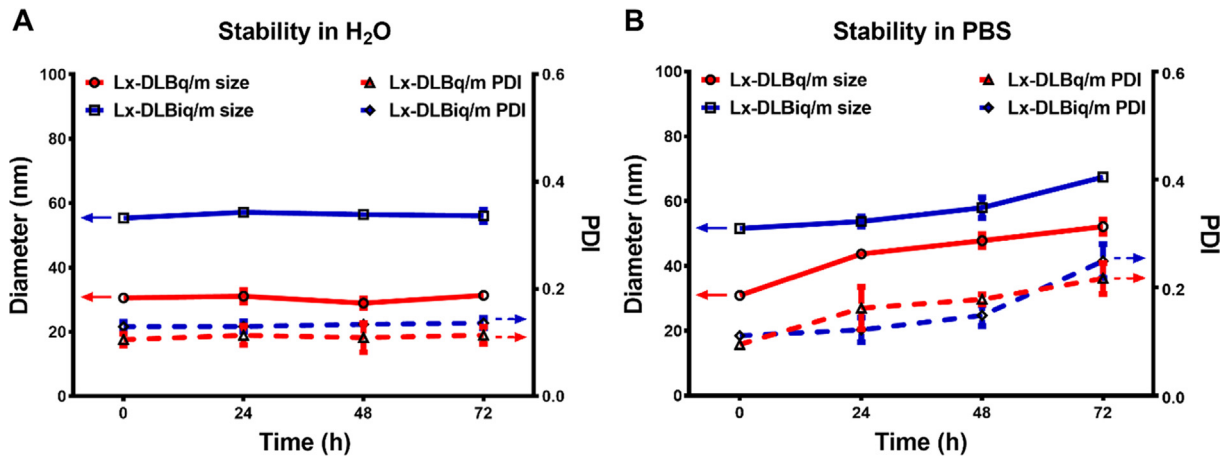

Fig. 4. Colloidal stability of Lx-DLB loaded micelles. (A) Hydrodynamic diameter and PDI of Lx-DLBq/m and Lx-DLBiq/m micelles in Milli Q H_2O at 37 °C for 72 h. Data are shown as mean ± S.D. (n = 3). (B) Hydrodynamic diameter and PDI of Lx-DLBq/m and Lx-DLBiq/m micelles in PBS at 37 °C for 72 h. Data are shown as mean ± S.D. (n = 3).

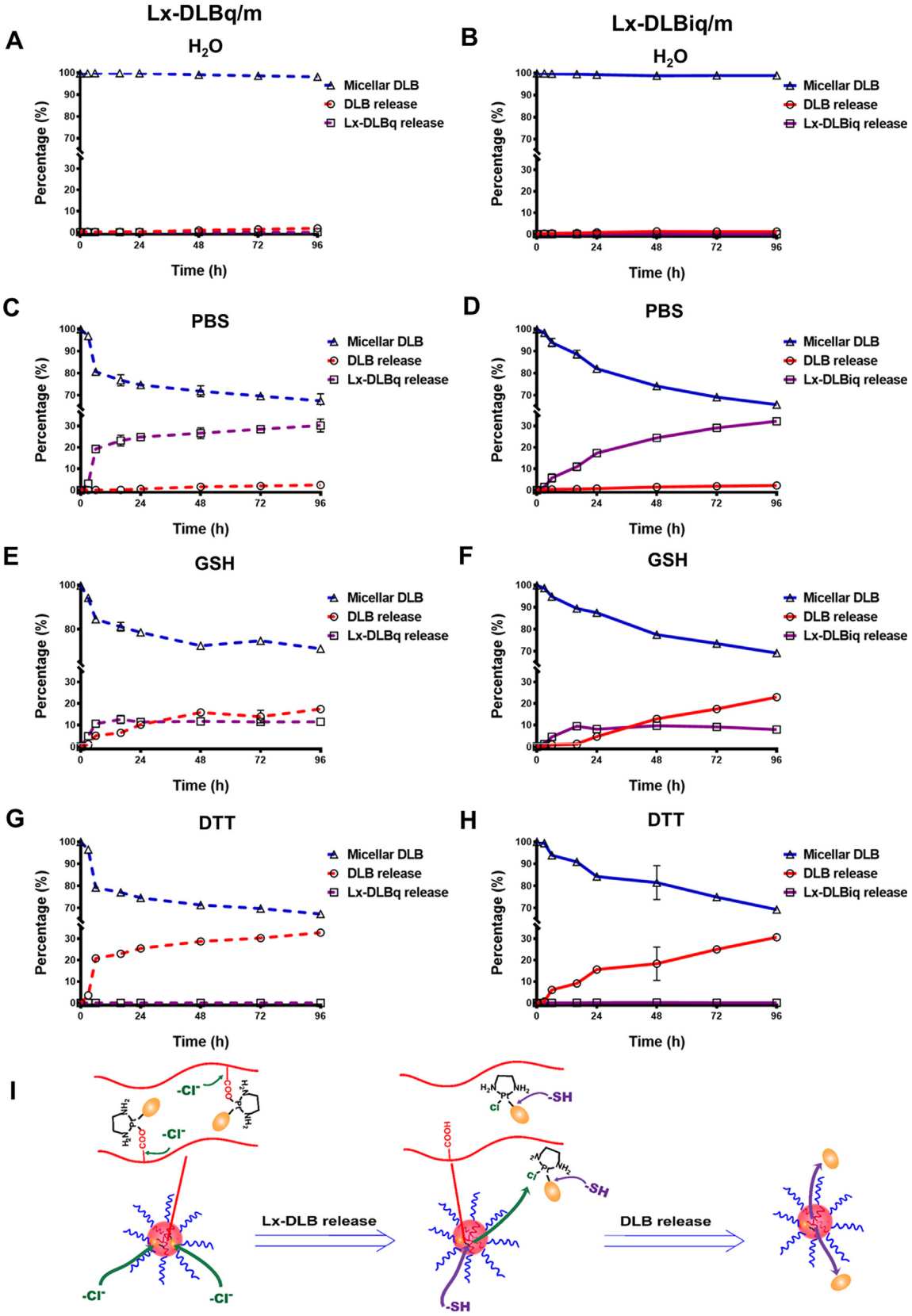

Fig. 5. Release profiles of DLB and Lx-DLBq from Lx-DLBq/m micelles (A, C, E and G) and from Lx-DLBiq/m micelles (B, C, F and H) upon incubation in H_2O, PBS, PBS containing 10 mM GSH and PBS containing 10 mM DTT for 96 h at 37 °C. All media contained 1% v/v Tween 80. The data are shown as the mean ± S.D. (n = 3). (I) Schematic representation of Lx-DLB and DLB release mechanism.

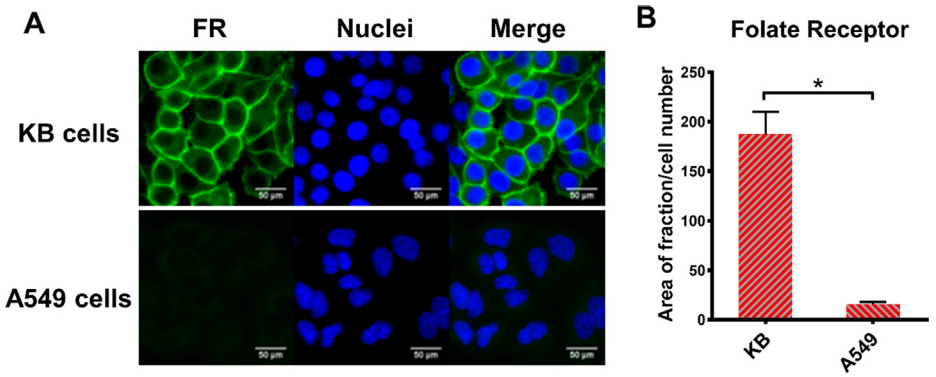

Fig. 6. (A) Immunostaining and quantification of the folate receptor on KB and A549 cells. IgG (H + L) Alexa Fluor 488 secondary antibody is stained in green and nuclei are stained in blue, bars 50 μm. (B) Relative area fraction of folate receptor as calculated by the software Image J. The data are shown as the mean ± S.D. (n = 3), * indicates $P < 0.05$.

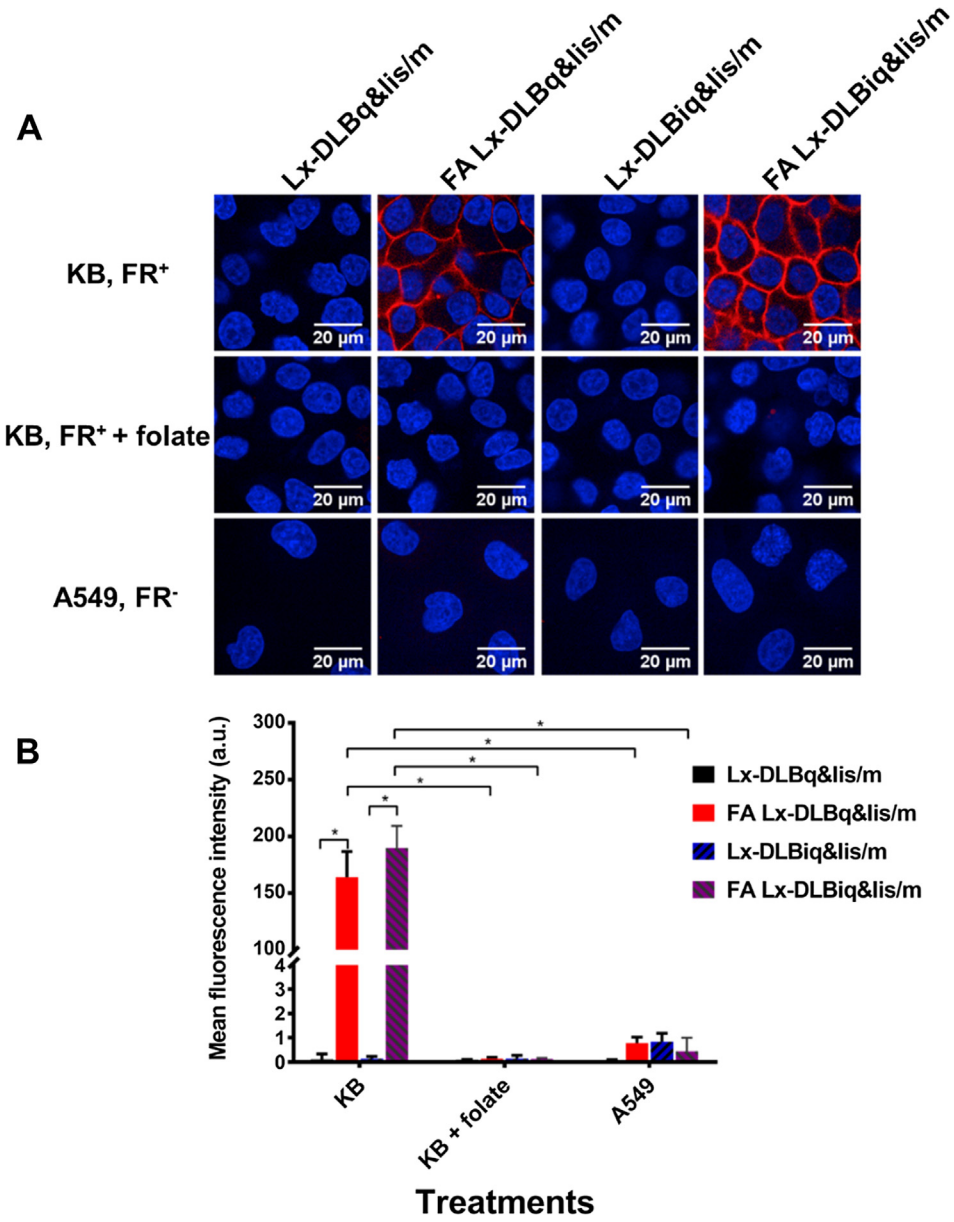

Fig. 7. Cellular binding of different micelles by KB and A549 cells. (A) Confocal microscopic images of KB cells and A549 cells incubated with Lx-DLB/Lx-Lis polymeric micelles (final concentrations were equivalent to 10 μM lissamine) for 1 h at 4 °C. Nuclei are stained in blue with Hoechst 33342 and lissamine is visible as red spots; size bars 20 μm. (B) Corresponding mean fluorescence intensity (MFI) calculated from the confocal images using ImageJ software. The data are shown as the mean ± S.D. (n = 3), * indicates $P < 0.05$.

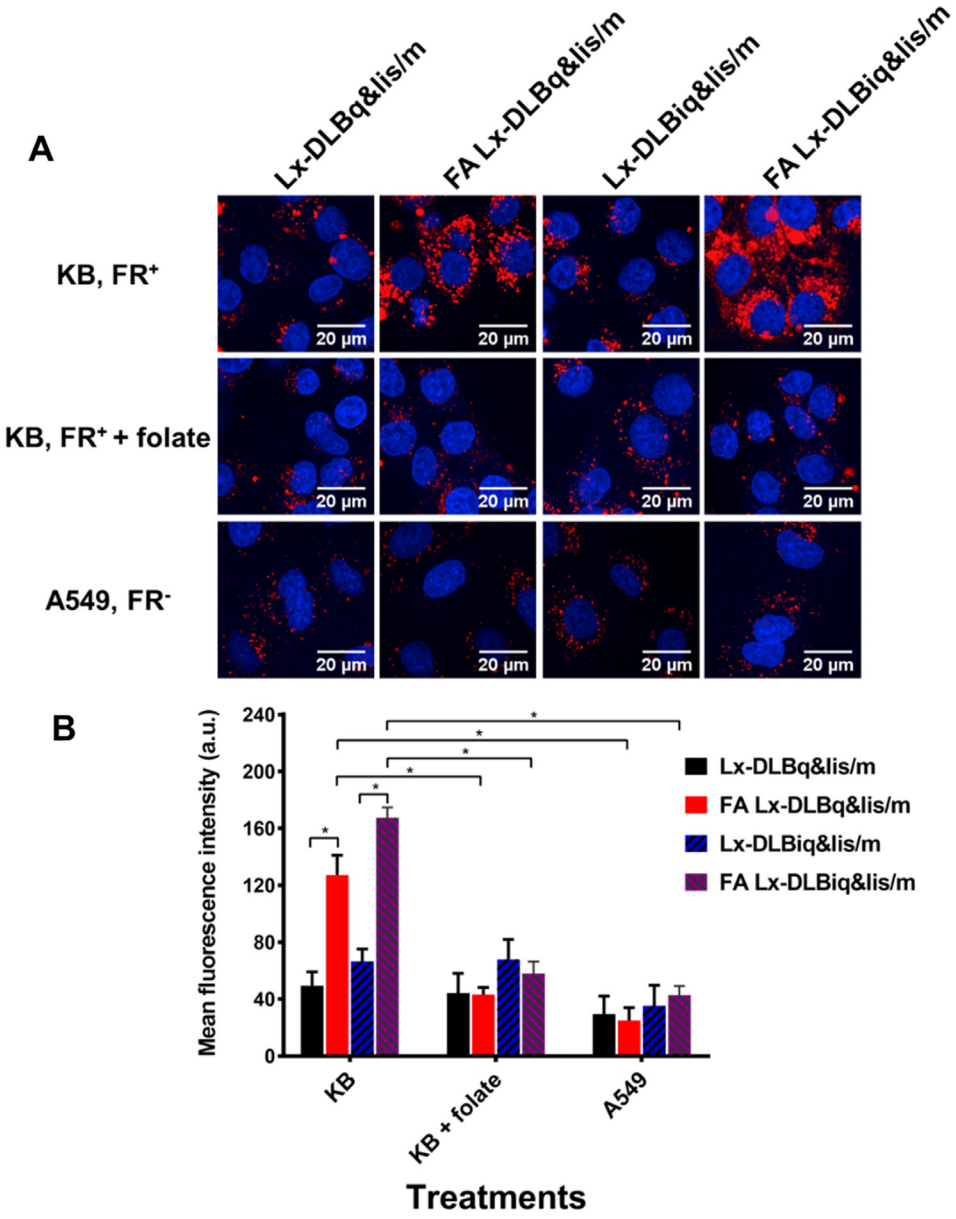

Fig. 8. Cellular uptake of different micelles by KB and A549 cells. (A) Confocal microscopic images of KB cells and A549 cells incubated with Lx-DLBq&lis/m, FA Lx-DLBq&lis/m, Lx-DLBiq&lis/m and FA Lx-DLBiq&lis/m micelles (the final concentrations were 10 μM equivalent lissamine) for 2 h at 37 °C. Nuclei are stained in blue with Hoechst 33342 and lissamine is visible as red spots, bars 20 μm. (B) The corresponding mean fluorescence intensity (MFI) calculated from the confocal images using ImageJ software. The data are shown as the mean ± S.D. (n = 3), * indicates $P < 0.05$.

The observed differences in inhibitory activity of DLB versus mTOR and PI3K are in good agreement with studies by other groups (see for instance Serra et al., 2008). Importantly, the inhibitory effect of folate targeted micelles could be blocked by an excess of free folate and non-folate control micelles did not display inhibitory activity. These results are in good agreement with the results on internalization of micelles (Fig. 8) and demonstrate that cellular uptake of micelles is required to reach effective levels of DLB in target cells.

Lastly, we determined cytotoxic effects of DLB and DLB loaded micelles in KB cells and A549 cells. DLB has potent antitumor effects and induces a range of antiproliferative and apoptotic effects in tumor cells such as cell-cycle arrest, invasion and migration (Maira et al., 2008; Serra et al., 2008; Shi et al., 2018). In the present study, we investigated the overall cytotoxicity and focused on the cellular specificity of folate targeted micelles by comparing cytotoxic effects in folate receptor-positive cells (i.e. KB cells) and folate receptor negative cells (i.e. A549 cells). Fig. 10 shows dose response curves after incubation with DLB or micellar formulations for 72 h (Panel A, B: KB cells; panel C and D: A549 cells). IC_{50} values of the treatments are listed in Table 3. Free DLB inhibited cellular viability similarly in both cell lines, with IC_{50} of 42 ± 6 and 37 ± 5 nM for KB and A549 respectively. Control micelles exhibited cytotoxic effects in A549 cells with IC_{50} values ranging from 430 to 640 nM, corresponding to relative activities of free DLB of 0.06–0.09 (6–9% versus free DLB). Since PEGylated micelles are not extensively internalized (Fig. 8), the reduction in antiproliferative effect is expected and roughly corresponds to the percentage of free DLB that becomes available for cellular uptake during the time course of the experiment. Fig. 5 shows that approximately 20% of total DLB (Lx-DLB plus DLB) is released in PBS or PBS with 10 mM glutathione (Fig. 5C–F) during three days. Although Lx-DLB is more hydrophilic than free DLB, it seems plausible that such a low molecular weight compound can cross the cellular membrane by passive diffusion, allowing its intracellular processing into bioactive DLB.

Folate decorated micelles and control micelles showed distinctive

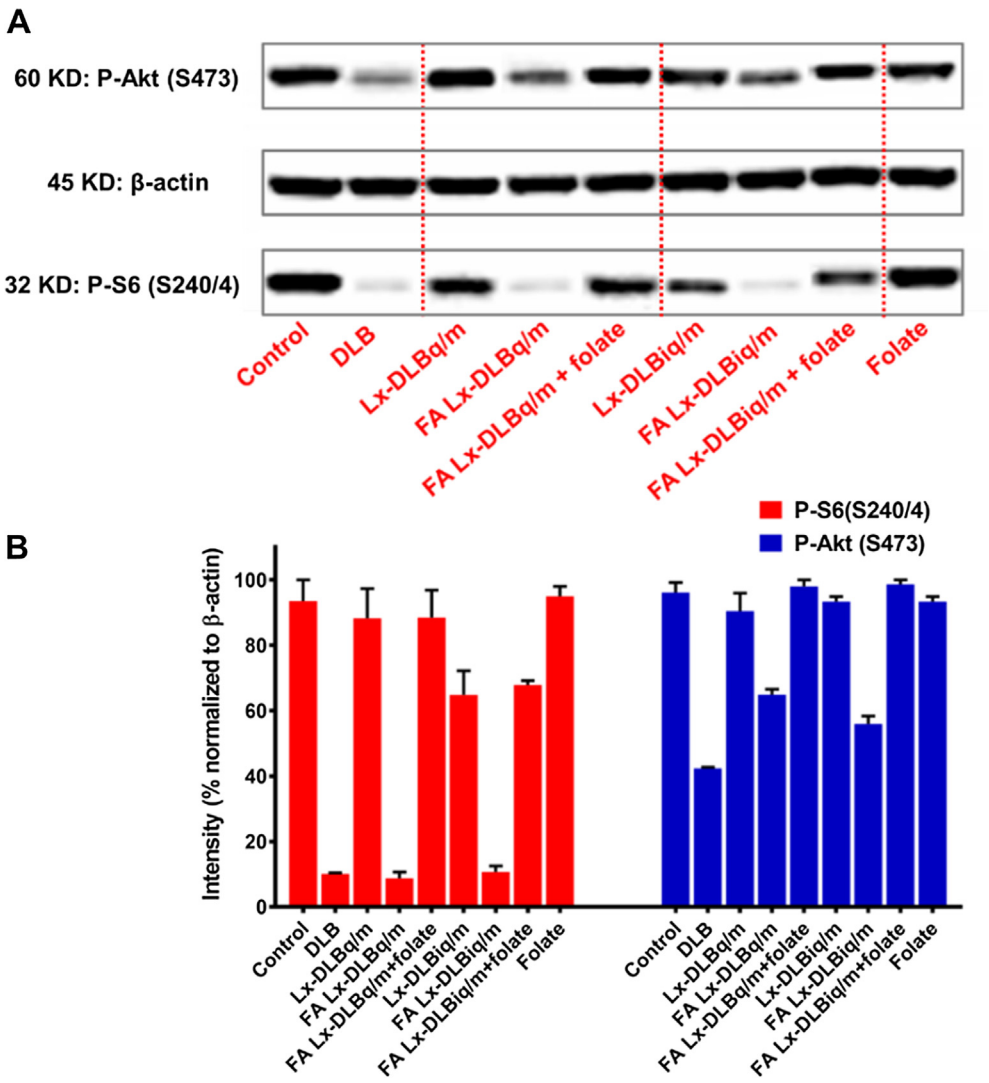

Fig. 9. Inhibition of PI3K and mTOR signaling pathways by DLB loaded polymeric micelles. KB cells were incubated with either free DLB (80 nM) or DLB loaded polymeric micelles equivalent to 80 nM DLB for 16 h at 37 °C. PI3K activity was determined by Western blot analysis of phosphorylated Akt (Ser473); mTOR activity was determined by Western blot analysis of phosphorylated S6 protein (Ser 240/244). Uptake of folate decorated micelles was inhibited by coincubation with excess free folate. (A) Representative Western blot bands of phosphorylation of Akt (Ser473) and S6 protein (Ser 240/244) after incubation of KB cells with free DLB and micellar formulations. β-Actin expression was analyzed as a loading control. (B) Semiquantitative analysis of P-S6 and P-Akt bands normalized to β-Actin bands. Data are presented as mean ± S.D. of two independent experiments.

differences in cytotoxic activity in KB cells. While folate targeted micelles displayed activity in the same range as free DLB (IC_{50} 48–73 nM, corresponding to 0.58–0.88 relative activity of free DLB), control micelles without folate tethers exhibited 3.4 fold lower activity (IC_{50} 157–250 nM, corresponding to 0.17–0.27 relative activity of free DLB). The selectivity of FR-mediated uptake pathway was confirmed once again by competition with excess free folate (Fig. 10B). Specific cell inhibitory activity of the FA-decorated micelles (added at 320 nM DLB concentration) was blocked by 100-fold molar excess folate (Fig. 10B). These *in vitro* cytotoxicity results are in good agreement with the studies on uptake and inhibition of mTOR/PI3K signaling, demonstrating that folate decorated micelles display selectivity for cells that overexpress folate receptors. When comparing the micelles prepared with the two different regio-isomers of Lx-DLB, we conclude that differences in micellar properties did not result in big differences in cellular activity, since the overall cellular uptake and cytotoxic activity are similar.

4. Conclusions and perspective

In conclusion, we have developed a novel type of polymeric micelles in which the drug is linked via platinum(II) coordination chemistry to the hydrophobic core of the micelles. Poly(ethylene glycol)-*b*-poly(acrylic acid) (PEG-*b*-PAA) block copolymers were reacted with Lx-DLB yielding amphiphilic drug-polymer conjugates that self-assembled into polymeric micelles. Surface-decoration of the polymeric micelles with folate targeting ligands yielded micelles that accumulated in target cells via folate receptor mediated endocytosis. Although size and shape of DLB loaded micelles differed depending on the type of regio-isomer of Lx-DLB, no major differences were observed in cellular activities of these products. *In vitro* cellular activity of DLB micelles strongly depended on receptor mediated endocytosis by folate receptor expressing cells. Our results support the further development of platinum-linked micellar formulations and their testing in preclinical animal models. Of note, it will be especially interesting to evaluate pharmacokinetic properties, to obtain evidence of their stability during their circulation in the blood stream, and their capability to deliver potent signal transduction inhibitors to tumors and into cancer cells.

CRediT authorship contribution statement

Haili Shi: Funding acquisition, Conceptualization, Methodology, Investigation, Formal analysis, Validation, Project administration, Visualization, Writing - original draft. **Mies J. van Steenbergen:** Conceptualization, Methodology, Validation, Formal analysis, Data curation. **Bo Lou:** Conceptualization, Methodology, Validation, Formal analysis, Data curation. **Yanna Liu:** Conceptualization, Methodology, Validation, Formal analysis, Data curation. **Wim E. Hennink:** Conceptualization, Supervision, Funding acquisition, Writing - review & editing. **Robbert J. Kok:** Conceptualization, Supervision, Funding acquisition, and Writing - review & editing.

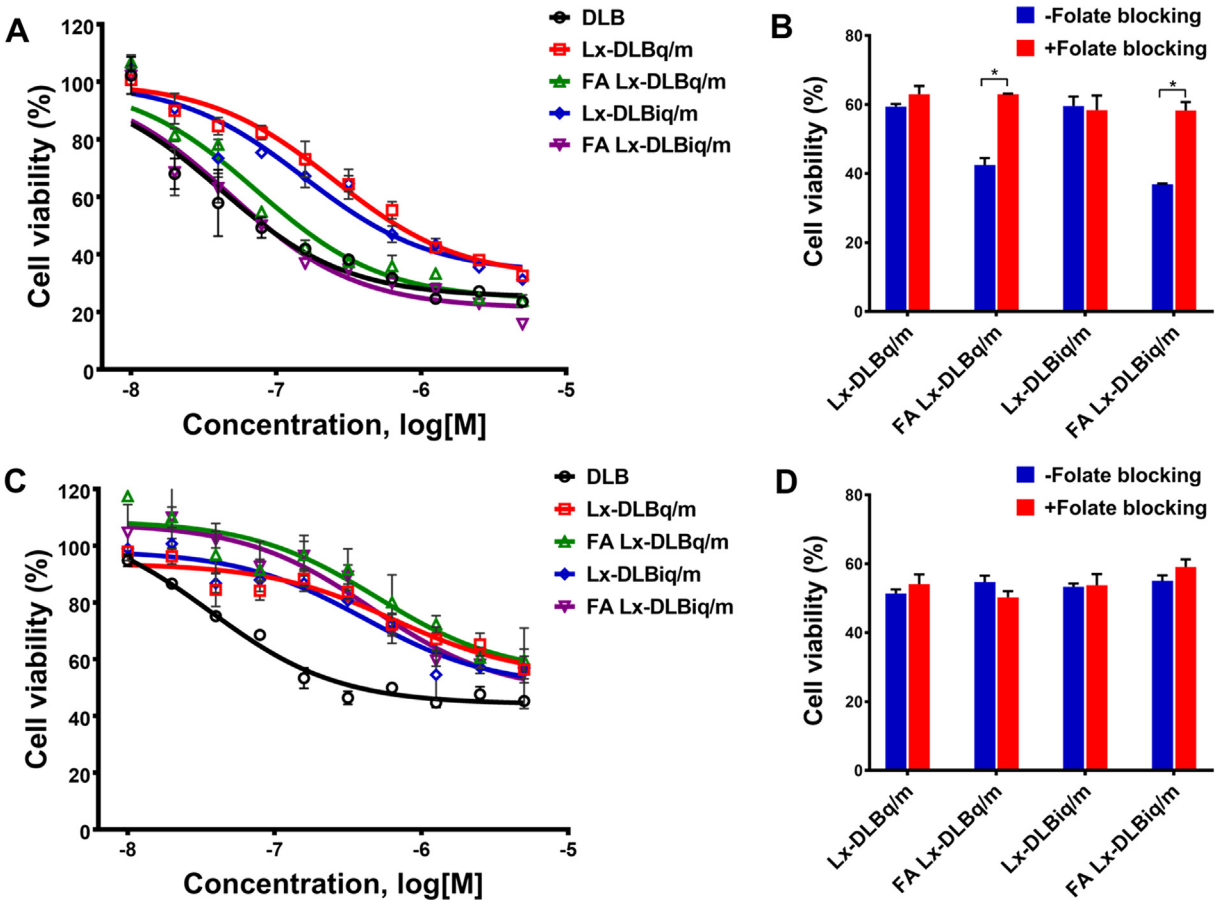

Fig. 10. Cytotoxic activity of DLB loaded polymeric micelles. All conditions were tested in triplicate. (A) Dose response curves of DLB formulations in KB cells after incubation for 72 h at 37 °C. (B) Cell viability of KB cells after incubation with micelles at a dose equivalent to 60% inhibition (i.e. corresponding to 320 nM DLB) with/without excess folate for 72 h at 37 °C (*$P < 0.05$). (C) Dose response curves of DLB formulations in A549 cells after incubation for 72 h at 37 °C. (D) Cell viability of A549 cells after incubation with a dose equivalent to 60% inhibition (i.e. corresponding to 5120 nM DLB) with/without excess folate for 72 h at 37 °C.

Table 3
IC_{50} values of dactolisib treatments in KB and A549 cells.

Treatment	IC_{50} in KB cells	Relative activity in KB cellsIC_{50} (free DLB)/ IC_{50} product	Folic acid targeting activity in KB cells IC_{50}(Control)[a]/IC_{50}(product)	IC_{50} in A549 cells	Relative activity in A549 cells IC_{50} (free DLB)/IC_{50} product
Free DLB	42 ± 6	n.a	n.a.	37 ± 5	n.a.
Control micelles Lx-DLBq/m	250 ± 11	0.17	n.a.	640 ± 274	0.06
FA decorated micelles FA Lx-DLBq/m	73 ± 1	0.58	3.4	543 ± 302	0.07
Control micelles Lx-DLBiq/m	157 ± 41	0.27	n.a.	430 ± 190	0.09
FA decorated micelles FA Lx-DLBiq/m	48 ± 7	0.88	3.3	477 ± 72	0.08

n.a. not applicable
[a] IC_{50}(Control) is the IC_{50} of the corresponding LX-DLB control micellar formulation.

Declaration of Competing Interest

The authors declare that they have no known competing financial interests or personal relationships that could have appeared to influence the work reported in this paper.

Acknowledgements

This work is supported by the China Scholarship Council (CSC). We thank Niels J. Sijbrandi from LinXis B.V. Pharmaceuticals for his scientific support about the synthesis of Lx-drug/dye. We thank Remco Fokkink from Wageningen University for the help with SLS measurement.

Appendix A. Supplementary material

Supplementary data to this article can be found online at https://doi.org/10.1016/j.ijpharm.2020.119305.

References

Ahn, J., Miura, Y., Yamada, N., Chida, T., Liu, X., Kim, A., Sato, R., Tsumura, R., Koga, Y., Yasunaga, M., Nishiyama, N., Matsumura, Y., Cabral, H., Kataoka, K., 2015. Antibody fragment-conjugated polymeric micelles incorporating platinum drugs for targeted therapy of pancreatic cancer. Biomaterials 39, 23–30.

Alani, A.W., Bae, Y., Rao, D.A., Kwon, G.S., 2010. Polymeric micelles for the pH-dependent controlled, continuous low dose release of paclitaxel. Biomaterials 31, 1765–1772.

Bae, Y., Fukushima, S., Harada, A., Kataoka, K., 2003. Design of Environment-Sensitive Supramolecular Assemblies for Intracellular Drug Delivery: Polymeric Micelles that are Responsive to Intracellular pH Change. Angew. Chem. Int. Ed. 42, 4640–4643.

Basolo, F., 1996. Recollections of early studies on platinum(II) complexes related to Chatt's contributions to coordination chemistry. Coord. Chem. Rev. 154, 151–161.

Brülisauer, L., Gauthier, M.A., Leroux, J.-C., 2014. Disulfide-containing parenteral delivery systems and their redox-biological fate. J. Control. Release 195, 147–154.

Buwalda, S., Nottelet, B., Bethry, A., Kok, R.J., Sijbrandi, N., Coudane, J., 2019. Reversibly core-crosslinked PEG-P(HPMA) micelles: Platinum coordination chemistry for competitive-ligand-regulated drug delivery. J. Colloid Interface Sci. 535, 505–515.

Cabral, H., Kataoka, K., 2014. Progress of drug-loaded polymeric micelles into clinical studies. J. Controll. Rel. Off. J. Controll. Rel. Soc. 190, 465–476.

Cabral, H., Matsumoto, Y., Mizuno, K., Chen, Q., Murakami, M., Kimura, M., Terada, Y., Kano, M.R., Miyazono, K., Uesaka, M., Nishiyama, N., Kataoka, K., 2011. Accumulation of sub-100 nm polymeric micelles in poorly permeable tumours depends on size. Nat. Nanotechnol. 6, 815–823.

Cabral, H., Miyata, K., Osada, K., Kataoka, K., 2018. Block copolymer micelles in nanomedicine applications. Chem. Rev. 118, 6844–6892.

Cabral, H., Nishiyama, N., Okazaki, S., Koyama, H., Kataoka, K., 2005. Preparation and biological properties of dichloro(1,2-diaminocyclohexane)platinum(II) (DACHPt)-loaded polymeric micelles. J. Controll. Rel. Off. J. Controll. Rel. Soc. 101, 223–232.

Chao, D., Jiang, Y., Ru, C., Meng, F., Zhong, Z., 2012. Biodegradable polymeric micelles for targeted and controlled anticancer drug delivery: Promises, progress and prospects. Nano Today 7, 467–480.

Chen, G., Wang, L., Cordie, T., Vokoun, C., Eliceiri, K.W., Gong, S., 2015. Multi-functional self-fluorescent unimolecular micelles for tumor-targeted drug delivery and bioimaging. Biomaterials 47, 41–50.

Chen, H., Kim, S., He, W., Wang, H., Low, P.S., Park, K., Cheng, J.X., 2008. Fast Release of Lipophilic Agents from Circulating PEG-PDLLA Micelles Revealed by in Vivo Förster Resonance Energy Transfer Imaging. Langmuir Acs J. Surf. Colloids 24, 5213–5217.

Chen, M., Moad, G., Rizzardo, E., 2009. Thiocarbonylthio end group removal from RAFT-synthesized polymers by a radical-induced process. J. Polym. Sci., Part A: Polym. Chem. 47, 6704–6714.

Chen, Y., Tezcan, O., Li, D., Beztsinna, N., Lou, B., Etrych, T., Ulbrich, K., Metselaar, J.M., Lammers, T., Hennink, W.E., 2017. Overcoming multidrug resistance using folate receptor-targeted and pH-responsive polymeric nanogels containing covalently entrapped doxorubicin. Nanoscale 9, 10404–10419.

Chong, Y.K., Moad, G., Ezio Rizzardo, A., Thang, S.H., 2010. Thiocarbonylthio End Group Removal from RAFT-Synthesized Polymers by Radical-Induced Reduction. J. Polym. Sci., Part A: Polym. Chem. 47, 6704–6714.

Chu, B., Liu, T., 2000. Characterization of Nanoparticles by Scattering Techniques. J. Nanopart. Res. 2, 29–41.

Davis, M.E., Chen, Z., Shin, D.M., 2008. Nanoparticle therapeutics: an emerging treatment modality for cancer. Nat. Rev. Drug Discov. 7, 771.

Dolman, M., Van Dorenmalen, K., Pieters, E., Lacombe, M., Pato, J., Storm, G., Hennink, W., Kok, R.J., 2012. Imatinib-ULS-lysozyme: A proximal tubular cell-targeted conjugate of imatinib for the treatment of renal diseases. J. Control. Release 157, 461–468.

Dolman, M.E., Fretz, M.M., Segers, G.J., Lacombe, M., Prakash, J., Storm, G., Hennink, W.E., Kok, R.J., 2008. Renal targeting of kinase inhibitors. Int. J. Pharm. 364, 249–257.

Dolman, M.E., Harmsen, S., Storm, G., Hennink, W.E., Kok, R.J., 2010. Drug targeting to the kidney: Advances in the active targeting of therapeutics to proximal tubular cells. Adv. Drug Deliv. Rev. 62, 1344–1357.

Fairbanks, B.D., Gunatillake, P.A., Meagher, L., 2015. Biomedical applications of polymers derived by reversible addition–fragmentation chain-transfer (RAFT). Adv. Drug Deliv. Rev. 91, 141–152.

Fang, J., Nakamura, H., Maeda, H., 2011. The EPR effect: Unique features of tumor blood vessels for drug delivery, factors involved, and limitations and augmentation of the effect ☆. Adv. Drug Deliv. Rev. 63, 136–151.

Fretz, M.M., Dolman, M.E., Lacombe, M., Prakash, J., Nguyen, T.Q., Goldschmeding, R., Pato, J., Storm, G., Hennink, W.E., Kok, R.J., 2008. Intervention in growth factor activated signaling pathways by renally targeted kinase inhibitors. J. Controll. Rel. Off. J. Controll. Rel. Soc. 132, 200–207.

Germack, D.S., Wooley, K.L., 2010. RAFT-based synthesis and characterization of ABC vs. ACB triblock copolymers containing tert-butyl acrylate, isoprene and styrene blocks. Macromol. Chem. Phys. 208, 2481–2491.

Gholizadeh, S., Kamps, J.A.A.M., Hennink, W.E., Kok, R.J., 2018. PLGA-PEG nanoparticles for targeted delivery of the mTOR/PI3kinase inhibitor dactolisib to inflamed endothelium. Int. J. Pharm. 548, 747–758.

Gothwal, A., Khan, I., Gupta, U., 2016. Polymeric Micelles: Recent Advancements in the Delivery of Anticancer Drugs. Pharm. Res. 33, 1–22.

Greene, A.C., Zhu, J., Pochan, D.J., Jia, X., Kiick, K.L., 2011. Poly(Acrylic Acid-b-Styrene) Amphiphilic Multiblock Copolymers as Building Blocks for the Assembly of Discrete Nanoparticles. Macromolecules 44, 1942.

Harmsen, S., Dolman, M.E., Nemes, Z., Lacombe, M., Szokol, B., Pato, J., Keri, G., Orfi, L., Storm, G., Hennink, W.E., Kok, R.J., 2011. Development of a cell-selective and intrinsically active multikinase inhibitor bioconjugate. Bioconjug. Chem. 22, 540–545.

Henne, W.A., Kularatne, S.A., Hakenjos, J., Carron, J.D., Henne, K.L., 2013. Synthesis and activity of a folate targeted monodisperse PEG camptothecin conjugate. Bioorg. Med. Chem. Lett. 23, 5810–5813.

Houdaihed, L., Evans, J.C., Allen, C., 2017. Overcoming the Road Blocks: Advancement of Block Copolymer Micelles for Cancer Therapy in the Clinic. Mol. Pharm. 14, 2503–2517.

Hu, Q., Rijcken, C.J., Bansal, R., Hennink, W.E., Storm, G., Prakash, J., 2015. Complete regression of breast tumour with a single dose of docetaxel-entrapped core-cross-linked polymeric micelles. Biomaterials 53, 370–378.

Jones, S.K., Lizzio, V., Merkel, O.M., 2016. Folate Receptor Targeted Delivery of siRNA and Paclitaxel to Ovarian Cancer Cells via Folate Conjugated Triblock Copolymer to Overcome TLR4 Driven Chemotherapy Resistance. Biomacromolecules 17, 76–87.

Krzysztoń, R., Salem, B., Lee, D.J., Schwake, G., Wagner, E., Rädler, J.O., 2017. Microfluidic self-assembly of folate-targeted monomolecular siRNA-lipid nanoparticles. Nanoscale 9, 7442–7453.

Leamon, C.P., Reddy, J.A., 2004. Folate-targeted chemotherapy. Adv. Drug Deliv. Rev. 56, 1127–1141.

Li, D., Kordalivand, N., Fransen, M.F., Ossendorp, F., Raemdonck, K., Vermonden, T., Hennink, W.E., van Nostrum, C.F., 2015. Reduction-sensitive dextran nanogels aimed for intracellular delivery of antigens. Adv. Funct. Mater. 25, 2993–3003.

Liu, T.-J., Koul, D., LaFortune, T., Tiao, N., Shen, R.J., Maira, S.-M., Garcia-Echevrria, C., Yung, W.K.A., 2009. NVP-BEZ235, a novel dual phosphatidylinositol 3-kinase/mammalian target of rapamycin inhibitor, elicits multifaceted antitumor activities in human gliomas. Am. Assoc. Cancer Res. 8, 2204–2210.

Liu, X., Zhang, P., Rödl, W., Maier, K., Lächelt, U., Wagner, E., 2017. Toward Artificial Immunotoxins: Traceless Reversible Conjugation of RNase A with Receptor Targeting and Endosomal Escape Domains. Mol. Pharmac. 14, 0-0.

Müller, A., Burchard, W., 1995. Structure formation of surfactants in concentrated sulphuric acid: a light scattering study. Colloid Polym. Sci. 273, 866–875.

Maeda, H., Sawa, T.M.Y., Hori, K., Wu, J., 2000. Tumor vascular permeability and the EPR effect in macromolecular therapeutics: a review. J. Control. Release 65, 271–284.

Maira, S.-M., Stauffer, F., Brueggen, J., Furet, P., Schnell, C., Fritsch, C., Brachmann, S., Chene, P., De Pover, A., Schoemaker, K., 2008. Identification and characterization of NVP-BEZ235, a new orally available dual phosphatidylinositol 3-kinase/mammalian target of rapamycin inhibitor with potent in vivo antitumor activity. Mol. Cancer Ther. 7, 1851–1863.

Makino, J., Cabral, H., Miura, Y., Matsumoto, Y., Wang, M., Kinoh, H., Mochida, Y., Nishiyama, N., Kataoka, K., 2015. cRGD-installed polymeric micelles loading platinum anticancer drugs enable cooperative treatment against lymph node metastasis. J. Control. Rel. Off. J. Controll. Rel. Soc. 220, 783–791.

van der Meel, R., Oliveira, S., Altintas, I., Haselberg, R., van der Veeken, J., Roovers, R.C., Storm, G., Hennink, W.E., Schiffelers, R.M., Kok, R.J., 2012. Tumor-targeted Nanobullets: Anti-EGFR nanobody-liposomes loaded with anti-IGF-1R kinase inhibitor for cancer treatment. J. Controll. Rel. 159, 281–289.

Meng, F., Hennink, W.E., Zhong, Z., 2009. Reduction-sensitive polymers and bioconjugates for biomedical applications. Biomaterials 30, 2180–2198.

Miura, Y., Takenaka, T., Toh, K., Wu, S., Nishihara, H., Kano, M.R., Ino, Y., Nomoto, T., Matsumoto, Y., Koyama, H., 2013. Cyclic RGD-linked polymeric micelles for targeted delivery of platinum anticancer drugs to glioblastoma through the blood–brain tumor barrier. ACS Nano 7, 8583–8592.

Nishiyama, N., Kato, Y., Sugiyama, Y., Kataoka, K., 2001. Cisplatin-loaded polymer-metal complex micelle with time-modulated decaying property as a novel drug delivery system. Pharm. Res. 18, 1035–1041.

Novo, L., Mastrobattista, E., van Nostrum, C.F., Hennink, W.E., 2014. Targeted decationized polyplexes for cell specific gene delivery. Bioconjug. Chem. 25, 802–812.

Péraudeau, E., Cronier, L., Monvoisin, A., Poinot, P., Mergault, C., Guilhot, F., Tranoy-Opalinski, I., Renoux, B., Papot, S., Clarhaut, J., 2018. Enhancing tumor response to targeted chemotherapy through up-regulation of folate receptor α expression induced by dexamethasone and valproic acid. J. Control. Release 269, 36–44.

Philip Stewart, L., Sumith Anurasiri, K., 2009. Folate-targeted therapeutic and imaging agents for cancer. Curr. Opin. Chem. Biol. 13, 256–262.

Prakash, J., de Borst, M.H., Lacombe, M., Opdam, F., Klok, P.A., van Goor, H., Meijer, D.K., Moolenaar, F., Poelstra, K., Kok, R.J., 2008. Inhibition of renal rho kinase attenuates ischemia/reperfusion-induced injury. J. Am. Soc Nephrol. JASN 19, 2086–2097.

Reedijk, B.J., 2008. Metal-Ligand Exchange Kinetics in Platinum and Ruthenium Complexes. Platin. Met. Rev. 52, 2–11.

Serra, V., Markman, B., Scaltriti, M., Eichhorn, P.J., Valero, V., Guzman, M., Botero, M.L., Llonch, E., Atzori, F., Di Cosimo, S., Maira, M., Garcia-Echeverria, C., Parra, J.L., Arribas, J., Baselga, J., 2008. NVP-BEZ235, a dual PI3K/mTOR inhibitor, prevents PI3K signaling and inhibits the growth of cancer cells with activating PI3K mutations. Cancer Res. 68, 8022–8030.

Shi, F., Zhang, J., Liu, H., Wu, L., Jiang, H., Wu, Q., Liu, T., Lou, M., Wu, H., 2018. The dual PI3K/mTOR inhibitor dactolisib elicits anti-tumor activityin vitroandin vivo. Oncotarget 9, 706–717.

Shi, H., Leonhard, W.N., Sijbrandi, N.J., van Steenbergen, M.J., Fens, M.H.A.M., van de Dikkenberg, J.B., Toraño, J.S., Peters, D.J.M., Hennink, W.E., Kok, R.J., 2019a. Folate-dactolisib conjugates for targeting tubular cells in polycystic kidneys. J. Control. Release 293, 113–125.

Shi, H., Lou, B., van Steenbergen, M.J., Sijbrandi, N.J., Hennink, W.E., Kok, R.J., 2019b. Polymeric Micelles Employing Platinum(II) Linker for the Delivery of the Kinase Inhibitor Dactolisib. Part. Part. Syst. Char. 36, 1900236.

Shi, Y., Lammers, T., Storm, G., Hennink, W.E., 2017. Physico-Chemical Strategies to Enhance Stability and Drug Retention of Polymeric Micelles for Tumor-Targeted Drug Delivery. Macromol. Biosci. 17, 1600160.
Sijbrandi, N.J., Merkul, E., Muns, J.A., Waalboer, D.C., Adamzek, K., Bolijn, M., Montserrat, V., Somsen, G.W., Haselberg, R., Steverink, P.J., 2017. A novel platinum (II)–based bifunctional ADC linker benchmarked using 89Zr-desferal and auristatin F–conjugated trastuzumab. Cancer Res. 77, 257–267.
Srinivasarao, M., Low, P.S., 2017. Ligand-targeted drug delivery. Chem. Rev. 117, 12133–12164.
Sungwon, K., Yunzhou, S., Young, K.J., Kinam, P., Ji-Xin, C., 2010. Overcoming the barriers in micellar drug delivery: loading efficiency, in vivo stability, and micelle-cell interaction. Exp. Opin. Drug Deliv. 7, 49.
Talelli, M., Barz, M., Rijcken, C.J.F., Kiessling, F., Hennink, W.E., Lammers, T., 2015. Core-crosslinked polymeric micelles: Principles, preparation, biomedical applications and clinical translation. Nano Today 10, 93–117.
Talelli, M., Iman, M., Varkouhi, A.K., Rijcken, C.J.F., Schiffelers, R.M., Etrych, T., Ulbrich, K., van Nostrum, C.F., Lammers, T., Storm, G., Hennink, W.E., 2010. Core-crosslinked polymeric micelles with controlled release of covalently entrapped doxorubicin. Biomaterials 31, 7797–7804.
Temming, K., Lacombe, M., van der Hoeven, P., Prakash, J., Gonzalo, T., Dijkers, E.C., Orfi, L., Kéri, G., Poelstra, K., Molema, G., Kok, R.J., 2006. Delivery of the p38 MAPkinase Inhibitor SB202190 to Angiogenic Endothelial Cells: Development of Novel RGD-Equipped and PEGylated Drug− Albumin Conjugates Using Platinum (II)-Based Drug Linker Technology. Bioconjug. Chem. 17, 1246–1255.
Uchino, H., Matsumura, Y., Negishi, T., Koizumi, F., Hayashi, T., Honda, T., Nishiyama, N., Kataoka, K., Naito, S., Kakizoe, T., 2005. Cisplatin-incorporating polymeric micelles (NC-6004) can reduce nephrotoxicity and neurotoxicity of cisplatin in rats. Br. J. Cancer 93, 678–687.
Ulbrich, K., Etrych, T., Chytil, P., Pechar, M., Jelinkova, M., Rihova, B., 2004. Polymeric anticancer drugs with pH-controlled activation. Int. J. Pharm. 277, 63–72.
van Dam, G.M., Themelis, G., Crane, L.M., Harlaar, N.J., Pleijhuis, R.G., Kelder, W., Sarantopoulos, A., de Jong, J.S., Arts, H.J., van der Zee, A.G., Bart, J., Low, P.S., Ntziachristos, V., 2011. Intraoperative tumor-specific fluorescence imaging in ovarian cancer by folate receptor-alpha targeting: first in-human results. Nat. Med. 17, 1315–1319.
van der Meel, R., Vehmeijer, L.J.C., Kok, R.J., Storm, G., van Gaal, E.V.B., 2013. Ligand-targeted particulate nanomedicines undergoing clinical evaluation: Current status. Adv. Drug Deliv. Rev. 65, 1284–1298.
van Dijk, F., Teekamp, N., Post, E., Schuppan, D., Kim, Y.O., Zuidema, J., Steendam, R., Klose, M.H.M., Meier-Menches, S.M., Casini, A., Horvatovich, P.L., Sijbrandi, N.J., Frijlink, H.W., Hinrichs, W.L.J., Poelstra, K., Beljaars, L., Olinga, P., 2019. The anti-fibrotic potential of a sustained release formulation of a PDGFβ-receptor targeted rho kinase inhibitor. J. Control. Release 296, 250–257.
Varela-Moreira, A., Shi, Y., Fens, M.H., Lammers, T., Hennink, W.E., Schiffelers, R.M., 2017. Clinical application of polymeric micelles for the treatment of cancer. Mater. Chem. Front. 1, 1485–1501.
Vlahov, I.R., Leamon, C.P., 2012. Engineering folate-drug conjugates to target cancer: from chemistry to clinic. Bioconjug. Chem. 23, 1357–1369.
Wang, M., Miura, Y., Tsuchihashi, K., Miyano, K., Nagano, O., Yoshikawa, M., Tanabe, A., Makino, J., Mochida, Y., Nishiyama, N., Saya, H., Cabral, H., Kataoka, K., 2016. Eradication of CD44-variant positive population in head and neck tumors through controlled intracellular navigation of cisplatin-loaded nanomedicines. J. Controll. Rel. Off. J. Controll. Rel. Soc. 230, 26–33.
Wu, H., Shi, H., Zhang, H., Wang, X., Yang, Y., Yu, C., Hao, C., Du, J., Hu, H., Yang, S., 2014. Prostate stem cell antigen antibody-conjugated multiwalled carbon nanotubes for targeted ultrasound imaging and drug delivery. Biomaterials 35, 5369–5380.
Yang, H., Lou, C., Xu, M., Wu, C., Miyoshi, H., Liu, Y., 2011. Investigation of folate-conjugated fluorescent silica nanoparticles for targeting delivery to folate receptor-positive tumors and their internalization mechanism. Int. J. Nanomed. 6, 2023–2032.
Yuan, M., Mou, Q., Zhu, X., Yan, D., 2017. Small molecule nanodrugs for cancer therapy. Mater. Today Chem. 4, 26–39.
Zhang, C., Li, C., Liu, Y., Zhang, J., Bao, C., Liang, S., Wang, Q., Yang, Y., Fu, H., Wang, K., 2015. Gold Nanoclusters-Based Nanoprobes for Simultaneous Fluorescence Imaging and Targeted Photodynamic Therapy with Superior Penetration and Retention Behavior in Tumors. Adv. Funct. Mater. 25, 1314–1325.
Zhang, W., Bing, F., Walther, A., MüLler, A.H.E., 2009. Synthesis via RAFT Polymerization of Tadpole-Shaped Organic/Inorganic Hybrid Poly(acrylic acid) Containing Polyhedral Oligomeric Silsesquioxane (POSS) and Their Self-assembly in Water. Macromolecules 42, 2563–2569.